A FRAMEWORK TO ESTIMATE POWER OUTPUT AS A FUNCTION OF INPUT VIBRATION PARAMETERS FOR VIBRATION ENERGY HARVESTING

by

John Dale Heit

A thesis submitted to the faculty of
The University of Utah
in partial fulfillment of the requirements for the degree of

Master of Science

Department of Mechanical Engineering

The University of Utah

August 2014

The University of Utah Graduate School

STATEMENT OF THESIS APPROVAL

The thesis of **John Dale Heit**

has been approved by the following supervisory committee members:

Shad Roundy	, Chair	**05/07/14** Date Approved
Mark Minor	, Member	**5/07/14** Date Approved
Sanford Meek	, Member	**05/07/14** Date Approved

and by **Tim Ameel** , Chair/Dean of

the Department/College/School of **Mechanical Engineering**

and by David B. Kieda, Dean of The Graduate School.

ABSTRACT

A standard lumped parameter model for an inertial vibration energy harvester consists of a proof mass, spring, and damper(s). This model can also be described with a proof mass, viscous damping element for parasitic mechanical losses, and a generalized transducer that applies some force to the mass damper system. The transducer may contain restorative spring elements and energy extraction elements to harvest power. Currently the framework to relate vibration input to an optimal transducer architecture does not exist. Previous work has shown that for some inputs nonlinear transducer architectures can result in an increased power output.

This paper outlines a mathematical framework needed in order to find the optimal transducer architecture for a given vibration input. This framework defines the theoretical upper limit that any inertial transducer can harvest from a given vibration input in the presence of viscous mechanical damping. This framework is then applied to three cases of standard input types.

The first application is a single sinusoid input. The transducer architecture found is the expected result, a linear spring with matched resonance to the input, and an energy extraction element, that behaves as a linear viscous damper, with matched impedance to the mechanical damping. The second application of this framework is an input of two sinusoids both having equal magnitude but different frequencies. The resulting optimal transducer is dependent on the difference in the frequencies of the two signals. This

optimal transducer is often not realizable with a passive system, as it is inherently time dependent. For all cases of frequency separation between the two sinusoidal inputs, the upper limit for the energy generated is found to be twice that of a linear harvester tuned to the lower of the two frequencies.

The third application is for an input whose frequency changes linearly in time (i.e. a swept sinusoid). The optimal transducer architecture for this input is found to be completely time dependent. However for the case when the change in the input frequency is much slower than the period of the system, the transducer can be approximated by a linear spring whose stiffness changes in time.

TABLE OF CONTENTS

LIST OF FIGURES

LIST OF TABLES

LIST OF SYMBOLS

A .....Acceleration amplitude of the input vibration

b_m.....Linear viscous mechanical damper coefficient

E_1.....Energy generated at $n = 1$

E_{gen} .....Energy transduced to a useful form

E_{in} .....Energy into the system

E_n .....Energy generated by at any value $n \neq 1$

E_{out} .....Energy out of the system

E_{TD} .....Energy into the system by the time dependent force

f_n .....Natural frequency

f_0 .....Initial frequency for sinusoidal sweep

f_r .....Frequency rate of change for swept sinusoidal input

F_T .....Transducer force

$F(t)$ .....Input force (vibration source)

$f(t)$ .....Frequency as a function of time

g.....Integrand of the functional

G.....Systems sensitivity

J.....Power squared functional

J_{eff} .....Effective inertia

k.....Linear spring constant

K_{eff} .....Effective linear spring constant

n.....Factor difference between two frequencies

$P_{monitor}$.....Power required to monitor the frequency of the input

P_{RMS} .....RMS power output

Q.....Quality factor

t .....Time

T .....Period of the input vibration

TD .....Time dependent force

x_1 .....Position of the proof mass

x_2 .....Velocity of the proof mass

κ .....Least common factor between two periods

ω.....Angular velocity

ζ_m .....Mechanical damping ratio

ζ_e .....Electrical damping ratio

ζ_T .....Total damping ratio for the system

R.....Real numbers

$\mathbb{Z}$ .....Integers

$\star$ .....Critical path

ACKNOWLEDGEMENTS

I would like to thank my advisor, Dr. Shad Roundy, for his help, guidance and allowing me to pursue this interesting field of research. I would also like to thank Dr. Andrej Cherkaev, for his insight and aid.

CHAPTER 1

INTRODUCTION

Energy harvesting or energy scavenging is the practice of taking ambient energy such as thermal gradients, electromagnetic energy, or mechanical vibrations and converting this wasted energy into a useful form; such as storing an electric potential in a capacitor or battery for later use [1], [2]. Common devices for harvesting energy from these types of sources include using thermoelectrics such as the Seebeck effect for thermal gradients, photovoltaics for electromagnetic waves at or near the visual spectrum, and inertial mechanical resonators coupled with piezoelectrics or an electromagnetic transducer for mechanical vibrations [1], [3].

Recently, the harvesting of mechanical vibrations has been the focus of much research [1-15]. This research has three main areas of focus. First, is the transduction mechanism. In broad terms this is the portion of the harvester that converts the mechanical motion into an electric voltage. This is primarily accomplished through the use of electrostatic generators, electromagnetic generators, and piezoelectric materials [1], [4].

The second area of research is the power electronics. These are the electronics responsible for converting the AC output of the generator to a DC signal in order to store the energy in a capacitor or battery. Because of the coupling between the mechanical and electrical domains, the power electronics can be used and optimized for power storage

as well as to control and manipulate the dynamics in the mechanical domain [5]. The final research area in vibration energy harvesting is with the dynamics of the mechanical resonator. For an inertial generator, one that is excited through base excitation, the relative motion and velocity of the proof mass will determine the energy available for the transducer to convert and the power electronics to store. The dynamics of the proof mass can be greatly affected by the architecture of the transducer. An example of this is a linear system excited by a sinusoid. The relative motion between the proof mass and the base can dramatically change by adjusting the stiffness of the spring connecting the proof mass to the base. In the case of a more complex input such as a sinusoid with varying frequency (chirp) or in the presence of multiple sinusoids the relationship between power output and parameter coefficients is unclear. Moreover, it is not clear if a spring with a linear constitutive law is optimal for energy output of the transducer. Recently much work has explored the use of nonlinearities, specifically spring nonlinearities as a way to improve power output or robustness from complex, nonsingle sinusoidal inputs. [6] [7] [8] [9] [10] [11].

The primary use for vibration energy harvesting is as a power source for wireless sensors [3], [2]. Wireless sensor networks are mainly used to observe and monitor the environments of systems; such as temperature, pressure, humidity, or the presence of a chemical or compound. The versatility of wireless sensor networks gives a broad range of applications including industrial factories, transportation, and structural health monitoring. Another common application is environmental health monitoring which includes monitoring air pollution and water quality as well as the detection of forest fires and other natural disasters.

Installation of a wired network is extremely expensive for large projects such as bridges and buildings. For example, the total cost for installing a 350 channel structural health monitoring system on the Tsing Ma suspension bridge, located in Hong Kong, had a cost of over $8 million. The high cost of this system is attributed to the installation and maintenance expense for the wiring of the sensors [12]. Many other systems including buildings, aircraft, and industrial settings could benefit from a potential reduction in cost. This reduction in cost is especially prevalent when the sensors are being retrofitted to the structure they are monitoring.

In addition to lowering the initial cost for installing a sensor network, the ability to use a completely wireless system has many other benefits. One of these benefits is the capability to place sensors in locations that were once unavailable, being inaccessible such as in a pressurized vessel. Making the sensors of the network self-powered also allows sensors to be placed in locations that are impossible to access after their construction or too expensive to access after manufacturing. When compared to batteries as a power source for wireless sensors, vibration energy harvesters have two distinct advantages: their inherent indefinite life cycle and a reduction in ongoing costs to maintain the network.

Generally, vibration inputs can be modeled in two different ways, either as a stochastic input or a deterministic signal. For conciseness this work will only evaluate signals that can be modeled as deterministic. In general this work can be applied to input vibrations of both types. Deterministic signals themselves can be broken down into two more categories. The first are time invariant signals where neither the amplitude(s) nor the frequency(s) of the signal change with time. The second category consists of time dependent signals. These signals have either time dependent amplitudes, frequencies, or

both.

Much research and available products are linear mass-spring-damper systems. These systems are modeled with a restoring force that obeys Hooke's law [9], [10], [7], [13]. The mechanical damping of the system is modeled as linear viscous damping and the power transduction as usually either a piezoelectric or electromagnetic generator. This type of harvester, known as an inertial mass harvester, is well understood and has been assumed to be the optimal structure for a single sinusoidal input in current literature [6], [4], [9], [14], [15], [13].

In order to determine the transducer force that will maximize power output it is necessary to start with a simple one degree of freedom model. This model will allow exploration of the relationship between the vibration input to the system and the energy output for a general transducer force acting on the system. This relationship will be a function of the system parameters as well as input parameters. The power output from this optimal transducer will define the upper limit for power output for any inertial generator of this form subjected to the given vibration input.

The results of this model will then be applied to three types of inputs. The first input is a single sinusoid. The optimal transducer for this input is found to be a linear spring, resonant with the input, and a linear viscous damper, with matched impedance to the parasitic mechanical losses. This solution has been assumed to be the optimal transducer for a single sinusoidal input, but until now has yet to be explicitly shown. It has been shown that if the form of the transducer architecture is assumed to be a linear spring and damper, the coefficients match those found in this work. By finding this solution that matched a partially known solution, the framework was validated.

The second input explored is the sum of two sinusoids of the same amplitude and different frequencies. The results in this case show that the optimal transducer contains an inherently time dependent restoring force. From this, we can conclude that an active system can outperform a passive system for this type of input, with assumptions on the energy requirement for the active component. The power output for the optimal transducer was found to be twice that of a linear system harvesting from only the lower of the two frequency components.

The final vibration input that is examined is that of a single sinusoid with a time dependent frequency. This type of input is known as a swept sine or chirp. The resulting optimal transducer was found to be a linear viscous damper and approximated by a linear spring with a time dependent coefficient. The power output for this system was found to have the same expression as for a linear system, harvesting from a single sinusoid, when expressed using the damping coefficient. This equality does not hold if the power output is expressed using the damping ratio. A device was then built in order to match the optimal transducer result found for the swept sinusoid. To validate that this device matched the output of the framework, the restoring force and damping was characterized. From static and dynamic testing the restoring force was found to be linear, matching the result of the framework for the optimal transducer.

CHAPTER 2[1]

MODELING

2.1 Introduction

A simplistic, generic model for an inertial energy harvester, as shown in Figure 1, is a kinetic harvester with a generic transducer force, F_T, that acts on the proof mass. This generic transducer may contain both energy dissipative elements for power generation as well as energy conservative restoring elements. In general, the system is subject to a generic force input $F(t)$. The inherent mechanical losses that are found in any real system are approximated by a linear viscous damper described by a single coefficient b_m. This single degree of freedom system is characterized by a single displacement x. If the system is excited through base excitation, as is the normal case for an inertial generator, then $F(t)$ would be the mass, (m), multiplied by the base acceleration $A(t)$. In this case the displacement, x, is the relative distance between the proof mass and ground. This system is modeled by equation 1.

$$m\ddot{x} + b_m\dot{x} + F_T = F(t) \tag{1}$$

[1] Portions of this chapter are forthcoming in, Heit, J., Roundy, S., 2013. "A Framework to Find the Upper Bound On Power Output as a Function of Input Vibration Parameters." Proceedings of the ASME 2014 Conference on Smart Materials, Adaptive Structures and Intelligent Systems. SMASIS2014 (September 08-10, 2014, Newport, Rhode Island, USA) (Accepted)

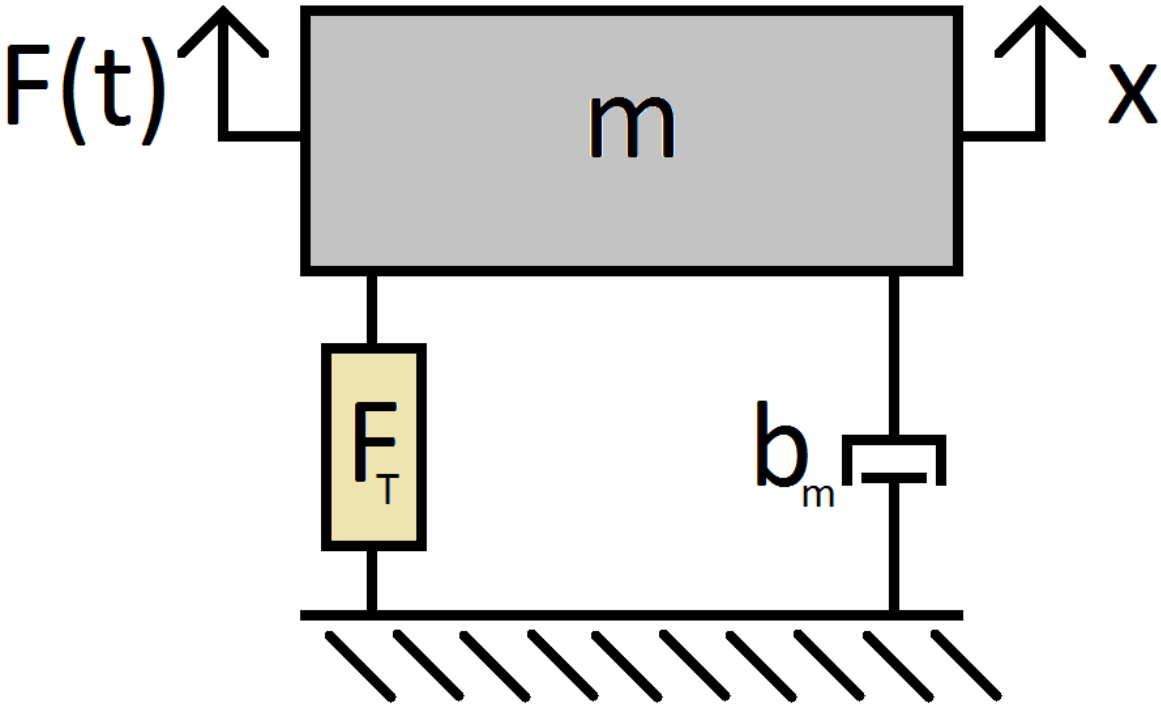

Figure 1. A generic inertial generator characterized by a single displacement x. Here F_T represents the force produced by an unknown transducer architecture. b_m is the coefficient that characterizes the system's linear viscous damping due to inherent mechanical losses of the system.

The second order differential equation 1 that models this generic system can be expressed in state space form by letting $x_1 = x, and\ x_2 = \dot{x}$:

$$\dot{x}_1 = x_2 \tag{2}$$

$$\dot{x}_2 = \frac{1}{m}\left(-b_m x_2 - F_T + F(t)\right) \tag{3}$$

2.2 Energy Balance

An energy balance of the system is used in order to find an expression for the energy generated by the transducer as a function of the input. By examining the energy balance of the system in steady state we can neglect the kinetic energy of the mass as well as the

possible potential energy stored in the transducer. This is due to the fact that these energy storage elements are restorative, thus they do not represent a net energy input or output to the system while it is in steady state.

$$E_{in} = E_{out} \tag{4}$$

$$E_{in} = \int F(t)x_2 \; dt \tag{5}$$

$$E_{out} \; = \int \; b_m x_2^2 \; dt + E_{gen} \tag{6}$$

Substituting equation 5 and 6 into 4 will yield an expression for the energy generated as a function of the input force and the velocity of the proof mass.

$$E_{gen} = \int [F(t)x_2 - b_m x_2^2] \; dt \tag{7}$$

For more generalized results we can look at the square of the energy to examine a continuous positive definite function thereby allowing us to find the critical points in the magnitude of the energy generated.

$$J = \; \int [F(t)x_2 - b_m x_2^2]^2 dt \tag{8}$$

2.3 Critical Points

We now have a properly formulated functional. If the velocity of the proof mass x_2 is treated as the control parameter, the critical points of the functional can be found through the stationary condition of the Euler-Lagrange equation [16]. Taking g to be the integrand

of equation 8 we have:

$$g = [F(t)x_2 - b_m x_2^2]^2 \ = F(t)^2 x_2^2 - 2b_m F(t) x_2^3 + b_m^2 x_2^4 \tag{9}$$

and the stationary condition to be:

$$\frac{\partial g}{\partial x_2} = 0 \tag{10}$$

For this application the stationary condition yields the critical points of the energy generated with respect to the velocity path of the proof mass. Equation 3 can be used to relate the velocity of the proof mass and the force of the transducer F_T acting on the proof mass. This relationship will allow an expression for the necessary transducer force so that the proof mass will follow the calculated optimal velocity path for energy generation. Solving the stationary condition for the critical velocities of x_2:

$$\frac{dg}{dx_2} = \ 2F(t)^2 x_2 - 6b_m F(t) x_2^2 + 4b_m^2 x_2^3 = 0 \tag{11}$$

$$(F(t) - 2b_m x_2)(F(t) - b_m x_2) x_2 = 0 \tag{12}$$

By factorization, the resulting three solutions are apparent. Here $\star$ denotes a critical path with respect to the energy generated.

$$x_2^\star = \frac{F(t)}{2b_m} \tag{13}$$

$$x_2^\star = \frac{F(t)}{b_m} \tag{14}$$

$$x_2^\star = 0 \tag{15}$$

These three relationships for $x_2^\star$ represent the critical velocity paths given a vibration input signal $F(t)$ to the system. This critical path, $x_2^\star$, will result in a minimum or maximum output of energy by the systems transducer. By substituting these signals into the second derivative the type of critical points are determined. The second derivative is found to be:

$$\frac{d^2g}{dx^2} = 2F(t)^2 - 12b_mF(t)x_2 + 12b_m^2x_2^2 \tag{16}$$

At $x_2^\star = \frac{F(t)}{2b_m}$:

$$\frac{d^2g}{dx^2} = 2F(t)^2 - 6F(t)^2 + 3F(t)^2 = -F(t)^2 \tag{17}$$

Which is negative for all input signals $F(t)$.

At $x_2^\star = \frac{F(t)}{b_m}$:

$$\frac{d^2g}{dx^2} = 2F(t)^2 - 12F(t)^2 + 12F(t)^2 = 2F(t)^2 \tag{18}$$

Which is positive for all input signals $F(t)$.

At $x_2^\star = 0$:

$$\frac{d^2g}{dx^2} = 2F(t)^2 \tag{19}$$

Which is positive for all input signals $F(t)$.

From this examination we can conclude that $x_2^\star = \frac{F(t)}{2b_m}$ corresponds to the maximum energy generated by the transducer for a given input force. While $x_2^\star = \frac{F(t)}{b_m} and\ x_2^\star = 0$ correspond to a minimum amount of energy generated. By substituting these relationships into the governing differential equations 2-3, an expression for the displacement of the proof mass x_1 as well as the transducer force F_T can be expressed as a function of the system properties and the input force.

For $x_2^\star = \frac{F(t)}{2b_m}$:

$$x_1^\star = \int \frac{F(t)}{2b_m} dt \tag{20}$$

$$\mathrm{F_T^\star} = -\frac{m\dot{F}(t)}{2b_m} + \frac{F(t)}{2} \tag{21}$$

Similarly for $x_2^\star = \frac{F(t)}{b_m}$:

$$x_1^\star = \int \frac{F(t)}{b_m} dt \tag{22}$$

$$F_T^\star = \frac{-m\dot{F}(t)}{b_m} \tag{23}$$

and for $x_2^\star = 0$

$$x_1^\star = 0 \tag{24}$$

$$F_T^\star = F(t) \tag{25}$$

Here, the transducer force F_T is an explicit function of time. The optimal transducer can then only be represented as a function of states if the input and its derivative can be expressed as a function of the states through the corresponding relationships of x_1 and x_2. These results are summarized in Table 1.

Table 1. Summary of critical path relationships for a generic input.

Critical Velocity Path	Critical Position Path	Critical Transducer Force	Type
$\mathbf{x_2^\star = \frac{F(t)}{2b_m}}$	$x_1^\star = \int \frac{F(t)}{2b_m} dt$	$F_T^\star = -\frac{m\dot{F}(t)}{2b_m} + \frac{F(t)}{2}$	Maximum
$\mathbf{x_2^\star = \frac{F(t)}{b_m}}$	$x_1^\star = \int \frac{F(t)}{b_m} dt$	$F_T^\star = -\frac{m\dot{F}(t)}{b_m}$	Minimum
$\mathbf{x_2^\star = 0}$	$x_1^\star = 0$	$F_T^\star = F(t)$	Minimum

CHAPTER 3

FIRST APPLICATION – SINGLE SINUSOID INPUT

3.1 Introduction

It is difficult to see the relevance of equations 20-23 in their general form. Equations 24 and 25 correspond to the trivial solution of a stationary condition of the proof mass. To help illustrate these relationships, shown in Table 1, a simple example of a single frequency sinusoidal input will be examined. This type of input is characterized by an amplitude and period that can be expressed though the angular velocity as shown in Figure 2. First we will examine the relationship that maximizes the energy output of the system, and then examine the conditions that create minimum energy output.

3.2 Critical Velocity, Position, and Transducer Paths

For the maximum power condition $x_2^\star = \frac{F(t)}{2b_m}$, letting $F(t) = A\ m\ sin(\omega t)$ results in the following relationships:

$$x_1^\star = -\frac{A\ m}{2b_m\omega}\cos(\omega t) \tag{26}$$

$$x_2^\star = \frac{A\ m}{2b_m}\sin(\omega t) \tag{27}$$

Figure 2. Example of a single sinusoid input, characterized by its amplitude and frequency.

$$F_T{}^{\star} = -\frac{A\,\omega\,m^2}{2b_m}\cos(\omega t) + \frac{A\,m}{2}\sin(\omega t) \tag{28}$$

Substituting for $x_1^{\star}\ and\ x_2^{\star}$ will yield the transducer force as a function of the systems states:

$$F_T^{\star} = \omega^2 m\, x_1 + b_m x_2 \tag{29}$$

Similarly for $x_2^{\star} = \frac{A\,m}{b_m}\sin(\omega t)$:

$$F_T^{\star} = \omega^2 m\, x_1 \tag{30}$$

and for $x_2^{\star} = 0$:

$$F_T^{\star} = F(t) \tag{31}$$

The three results for the critical transduction force can be interpreted as follows: for the maximizing condition, $x_2^\star = \frac{F(t)}{2b_m}$, the optimal transducer model, as shown in equation 29, is a linear spring, for a conservative restoring element, and a linear viscous damper for an electrical transducer. The constant of the linear spring is found to be resonant with the vibration input. The impedance of the electrical damper is found to be matched to the impedance of the mechanical damper. That is, b_m, from equations 1 and 3 is the same value as b_m for the transducer in equation 29. This system is a completely passive system, being only a function of the system's states. The system is shown in Figure 3 and modeled by the differential equation 32.

$$m\ddot{x} + 2b_m\dot{x} + kx = F(t) \tag{32}$$

3.3 Comparison to Previous Solutions

The result of a linear spring, with constant $k = \omega^2 m$, and linear viscous damping, with matched impedance, was the expected result that has been assumed in the literature but, until now, has yet to have been explicitly proven. Once a linear viscous damper element for the power generation has been assumed, the optimal power output can be shown to occur when these two impedance values match. This relationship can be shown through an analytical solution for the power output of a linear system with parasitic losses as in Figure 3 and equation 32. The relationship for the average power output from a linear system under a sinusoidal excitation of amplitude A and angular velocity ω is given by [4] and shown in equation 33. This relationship shows that the power output is inversely proportional to the input frequency.

Here, $\zeta_e \; and \; \zeta_m$ are the nondimensionalized damping ratios of the electrical

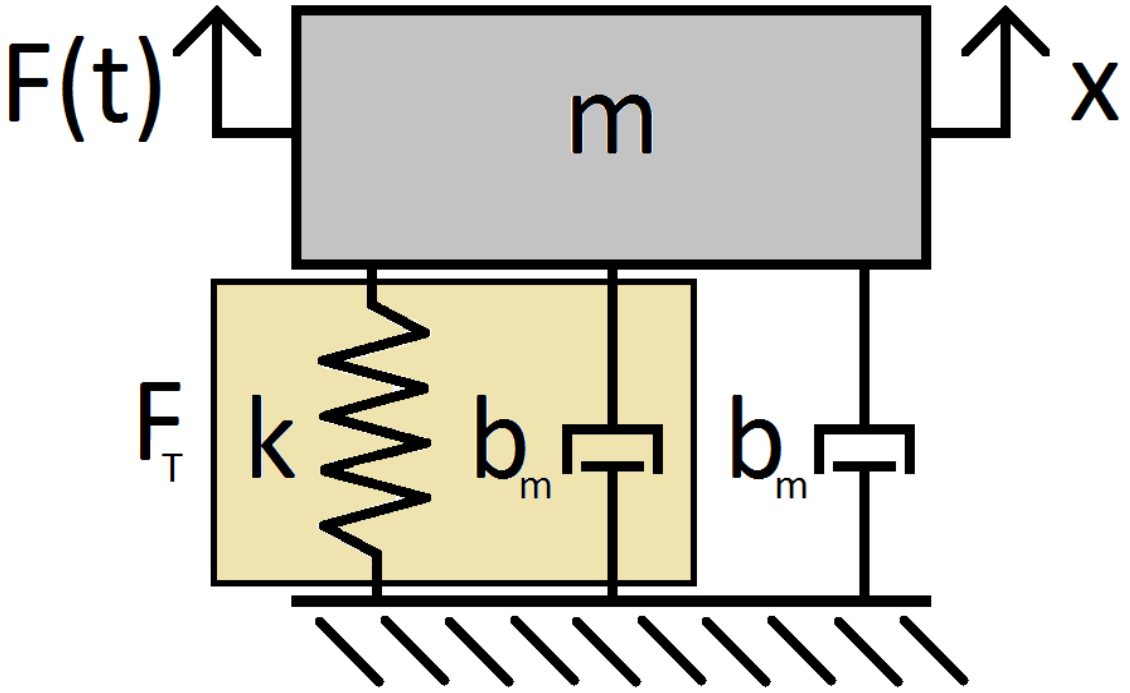

Figure 3. A diagram of the optimal power transducer architecture for an input $F(t) = A\,m\,sin(\omega t)$, where $k = \omega^2 m$.

transducer and mechanical damping from parasitic losses, respectively. ζ_T is the total damping of the system defined as $\zeta_T = \zeta_e + \zeta_m$. Differentiating the expression of the average power output with respect to ζ_e and setting equal to zero, the critical values of ζ_e can be determined.

$$P_{RMS} = \frac{m\zeta_e A^2}{4\omega\zeta_T^2} = \frac{m\zeta_e A^2}{\omega(\zeta_e + \zeta_m)^2} \tag{33}$$

$$\frac{dP_{RMS}}{d\zeta_e} = \frac{A^2 m}{4\omega(\zeta_e + \zeta_m)^2} - \frac{A^2 m\zeta_e}{2\omega(\zeta_e + \zeta_m)^3} = 0 \tag{34}$$

With a little algebra, it can be shown that equation 34 has only one nontrivial solution, when $\zeta_e = \zeta_m$. Looking at the second derivative for convexity gives:

$$\frac{d^2P_{RMS}}{d\zeta_e^2} = \frac{3A^2m\zeta_e}{2\omega(\zeta_e+\zeta_m)^4} - \frac{A^2m}{\omega(\zeta_e+\zeta_m)^3} \tag{35}$$

Evaluating at $\zeta_e = \zeta_m$:

$$\frac{d^2P_{RMS}}{d\zeta_e^2} = -\frac{A^2m}{32\omega\zeta_e^3} \tag{36}$$

which is negative for all A assuming $m > 0$, $\omega > 0$, and $\zeta_e > 0$, making $\zeta_e = \zeta_m$ the only maximum of the power output as a function of the electrical damping ζ_e. This relationship is shown in Figure 4 as the normalized power as a function of the ratio ζ_e/ζ_T.

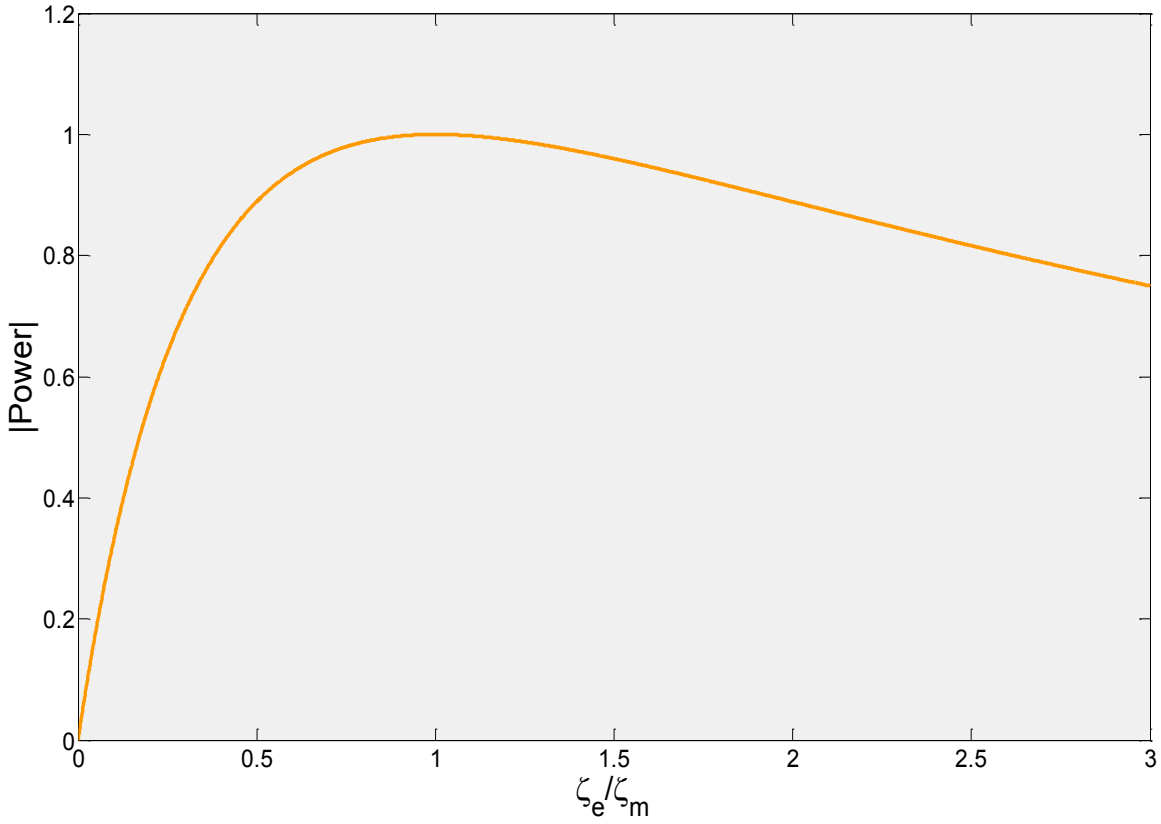

Figure 4. The normalized power output of a linear generator to a sinusoidal vibration input versus the ratio of damping due to electrical generation to mechanical loses. The maximum power output occurs when these two parameters are equal.

3.4 Interpretation of Minimum Solutions

For completeness we will examine the critical path $x_2^\star = \frac{A\,m}{b_m}\sin(\omega t)$, which corresponds to a minimum power condition. By using equations 22-25, and the state space equations 2-3 the corresponding transducer force is found to be a linear spring with spring constant $k = \omega^2 m$. This system is shown in Figure 5 and modeled by equation 37. While this system has a large response in x_1 to the input $F(t) = A\,m\,sin(\omega t)$, no energy will be converted to useful electric energy since the system's only dissipative element is from parasitic losses due to mechanical damping. The final relationship $x_2^\star = 0$ gives the trivial stationary solution for the energy output, as previously mentioned. Under this condition,

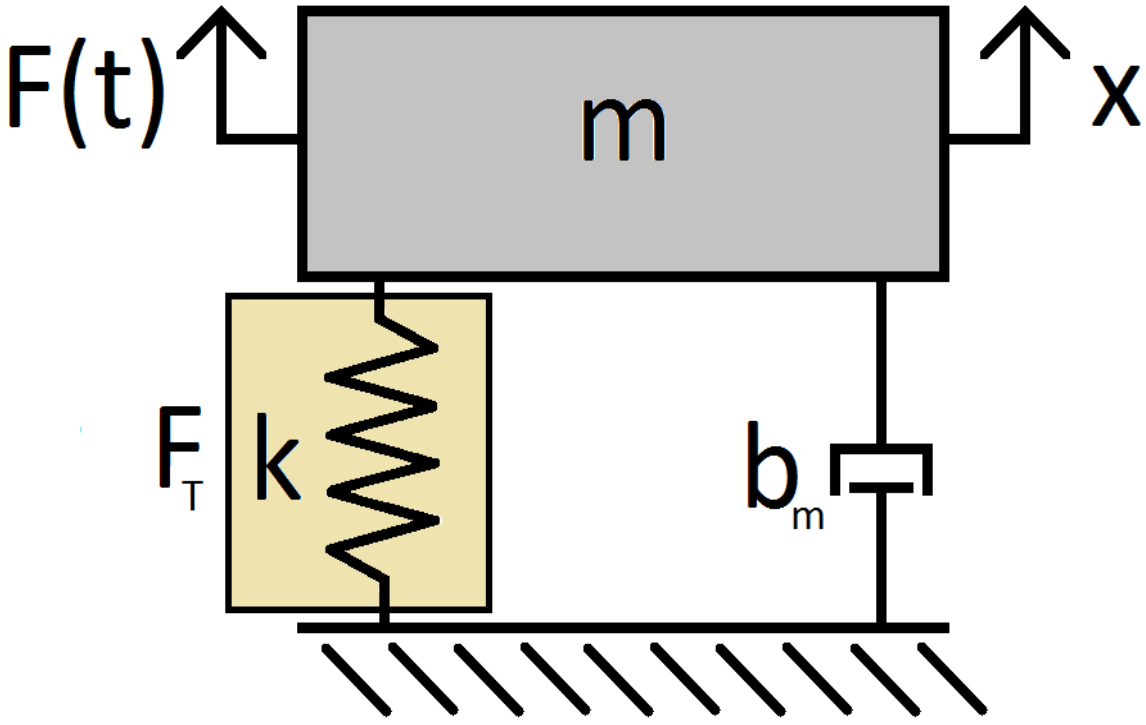

Figure 5. This diagram represents the transduction model for the minimum energy outputs for $x_2^\star = \frac{F(t)}{b_m}$ is $k = \omega^2 m$ and for $x_2^\star = 0$ is $k = \infty$.

the transducer force F_T provides an equal and opposite force to the input $F(t)$ on the mass in order to keep the proof mass stationary. In the case of base excitation, the relative displacement between the proof mass and ground is zero. Physically this would be accomplished by the use of an infinitely stiff spring for the transducer, $k = \infty$.

$$m\ddot{x} + b_m\dot{x} + kx = F(t) \tag{37}$$

3.5 Conclusion

This simple example of a single sinusoid input was used to validate the mathematical framework. The solution found for the maximum energy generation was one that has been assumed in the literature, but has yet to be analytically proven as the optimal solution. In addition to the maximum solution, two solutions corresponding to the minimum energy output were found. These two solutions corresponded to zero energy generated. The realizations of the two solutions are: a linear spring, resonant with the input vibration; and an infinitely stiff spring that allows for no relative displacement of the proof mass. Both of these solutions contained no energy dissipative elements for energy generation.

CHAPTER 4

SECOND APPLICATION – DOUBLE SINUSOID INPUT

4.1 Introduction

A common vibration input is one of two simultaneous sinusoids at different frequencies. This type of vibration occurs in rotating machinery where two unbalanced masses rotate at different rates fixed relative to one another or in a system where multiple harmonics of are well represented.

The average power output, as shown in equation 33, scales with A^2, where A is the amplitude of the acceleration vibration input, for the linearized system. Thus, the case where the amplitudes of the two sinusoids are equal will be examined. In the case where one sinusoid has an amplitude much greater than the other, it is reasonable to assume that the maximum power generation will be achieved by creating a linear harvester tuned to the ω corresponding to the maximum value of $\frac{A^2}{\omega}$. The expression for this double sinusoidal input is shown in equation 38.

$$F(t) = A\, m\, (\sin(\omega t) + \sin(n\omega t)) \tag{38}$$

Here, $n \in (1\ \infty)$ represents the multiple difference between the two frequency components. This analysis assumes that both frequency components are known a priori.

4.2 Critical Velocity, Position, and Transducer Paths

Examining now only the input-velocity relationship from equation 13 which results in the maximum energy output, the optimal velocity signal for an input of two sinusoids is obtained:

$$x_2^\star = \frac{A\,m}{2b_m}(\sin(\omega t) + \sin(n\omega t)) \tag{39}$$

Using equations 20 and 21 the relationships for the optimal position path and corresponding transducer force to achieve the velocity response as shown in equation 39 can be written as:

$$x_1^\star = -\frac{A\,m}{2\omega b_m}\left(\cos(\omega t) + \frac{1}{n}\cos(n\omega t)\right) \tag{40}$$

$$F_T^\star = \frac{A\,m}{2}\left(sin(\omega t) + sin(n\omega t)\right) - \frac{A\,\omega\,m^2}{2b_m}\left(cos(\omega t) + ncos(n\omega t)\right) \tag{41}$$

Substituting equations 40 and 41 for $x_1$and x_2 into equation 40, where available, yields:

$$F_T^\star = b_m x_2 + \omega^2 m\, x_1 + TD \tag{42}$$

where TD is the time dependent component of the transducer force that cannot be directly substituted for by the systems states $x_1 and\ x_2$.

$$TD = \frac{A\,\omega\,m^2}{2b_m}\left(\frac{1}{n} - n\right)\cos(n\omega t) \tag{43}$$

For the linear case, when $n = 1$, the amplitude of the time dependent portion of the

transducer is zero. This intuitive result for the transducer force shows that as $n \to 1$ the amplitude of the time dependent component goes to zero and the transducer architecture converges to the linear harvester as seen for the single sinusoidal input in equation 29. However, as $n \to 0$ or ∞ the amplitude of the time dependent portion of the transducer force grows without bound, as is shown in Figure 6. The time dependent component of the transducer force shows that the true unconstrained optimal transducer force for an input vibration of this form cannot be realized with a passive system; a system that is only a function of the states. This is due to the complex behavior of the optimal transducer force. In a single period of the proof mass, a different value of the optimal transducer force is required for the same values of the states.

Figure 6. The effect of n on the amplitude of the time dependent component of the transducer force.

This relationship is illustrated in Figure 7. This result shows that in principle an active system can outperform a passive system of any type, linear or nonlinear. However, this would assume that the restoring force implemented is conservative.

4.3 Conservation of Energy of the Time Dependent Component

To ensure that the energy balance of equation 4 holds, we must confirm that the time dependent component of the transducer is not an active component; doing net work on the system over time. That is, it must be a conservative or energy dissipative element, one that generates useful electric energy from the system. The net energy into the proof mass from the time dependent force can be calculated by integrating the force over the displacement for a period T of the entire signal.

$$E_{TD} = \int_0^T TD\, dx_1 = \int_0^T TD * x_2^{\star}\, dt \tag{44}$$

Substituting equation 43 and 39 for the time dependent portion of the transducer and optimal velocity path, respectivly, results in:

$$E_{TD}(t) = \frac{A^2 \omega m^3}{4b_m^2}\left(\frac{1}{n} - n\right)\int_0^T (\sin(\omega t)\cos(n\omega t) + \sin(n\omega t)\cos(n\omega t))dt \tag{45}$$

Evaluating this integral yields:

$$E_{TD}(T) = \frac{A^2 m^3 \begin{pmatrix} 1 + 2n - n^2 - 2n\mathrm{Cos}[T\omega]\mathrm{Cos}[nT\omega] + \\ (-1 + n^2)\mathrm{Cos}[nT\omega]^2 - 2n^2\mathrm{Sin}[T\omega]\mathrm{Sin}[nT\omega] \end{pmatrix}}{8\mathrm{b}_\mathrm{m}^2 n^2} \tag{46}$$

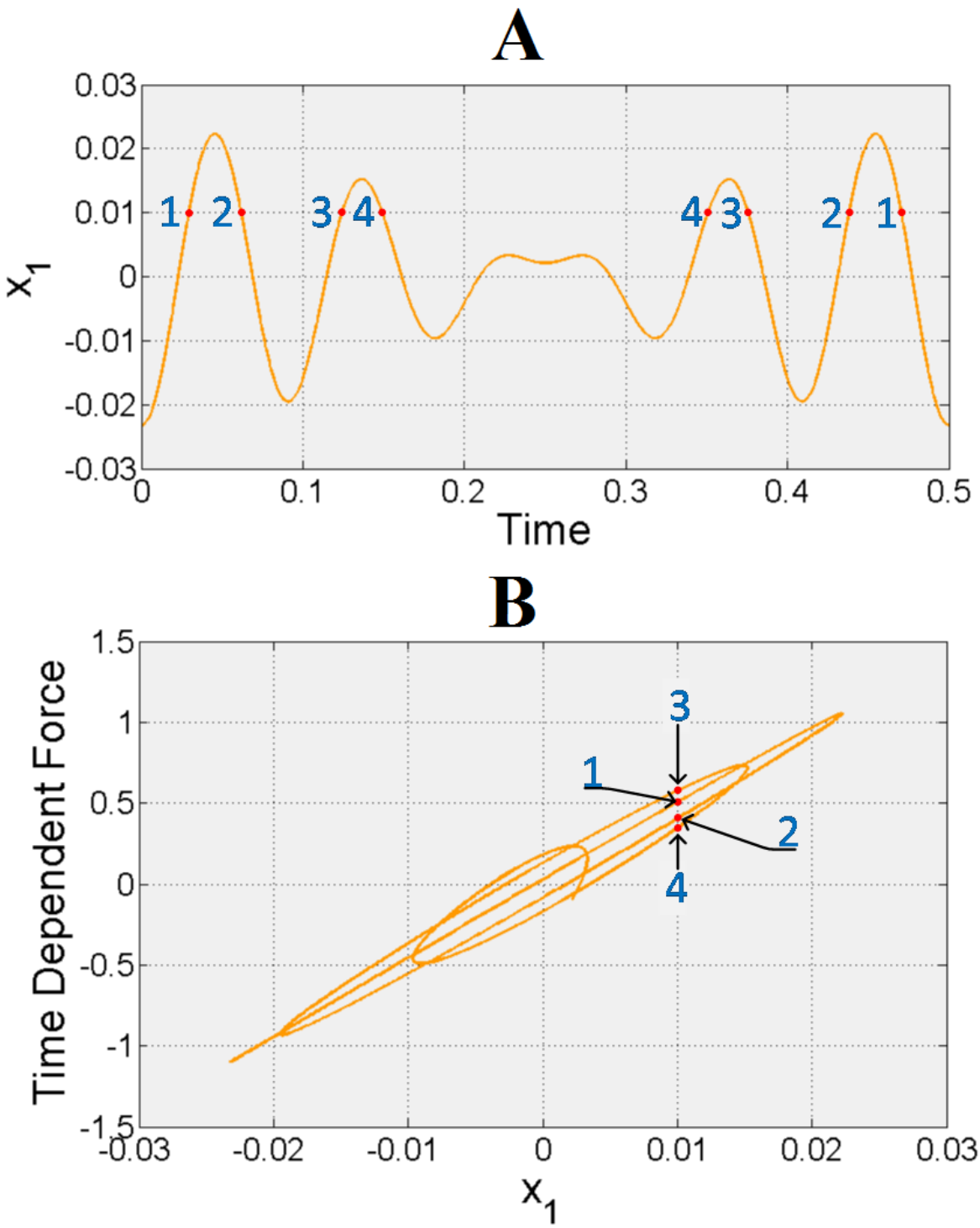

Figure 7. Phase portrait of the time dependent force. (A) The steady state position of the proof mass versus time for $n = 1.2$. This complex path repeats itself every period T of the input signal. (B) The time dependent force plotted over the optimal path x_1 over a period T. It can be seen that during one period the same position is repeated multiple times, but requires a different transducer force.

$$E_{TD}\left(\frac{2\pi}{\omega}\right) = -\frac{A^2 m^3(-1-2n+n^2+(-1+n^2)\text{Cos}[2n\pi])\text{Sin}[n\pi]^2}{4b_m^2 n^2} \quad (47)$$

Noting that for $n \in \mathbb{Z}$, $\sin(n\pi) = 0$ and $E_{TD}\left(\frac{2\pi}{\omega}\right) = 0$, where $\mathbb{Z}$ is the set of all integers. This shows that for $n \in \mathbb{Z}$ the net energy from the time dependent force into the system over a period T is zero. That is to say that the transducer can apply the time dependent force to the system without a net energy flow into the system. An example of this type of input with $n \in \mathbb{Z}$ can be seen in Figure 8.

For the general case, when $n \in R_{>1}$, where $R_{>1}$ is the set of all real numbers greater than 1, the period of the input signal is not trivial to find and can even be infinite in the case when n is an irrational number or has a nonterminating decimal place such as $n = \frac{4}{3}$.

We can define the period of the total signal by examining when the two portions of the signal intersect the origin. This can be found by checking when the product $n * \kappa$ is an integer, where $\kappa \in \mathbb{Z}^+$. For every value of κ where the value $n * \kappa$ is an integer, both components of the input signal are zero and have completed a full period. The period of the input vibration can then be found by:

$$T = \frac{2\pi}{\omega} * \kappa \quad (48)$$

where the value of κ used is the smallest positive integer, such that $n * \kappa$ is an integer value. This relationship is best explained and visualized through example input signals.

For $n = 1.2$, the smallest value of κ such that $n * \kappa$ is an integer value is $\kappa = 5$. So, the period of the total signal is describes as:

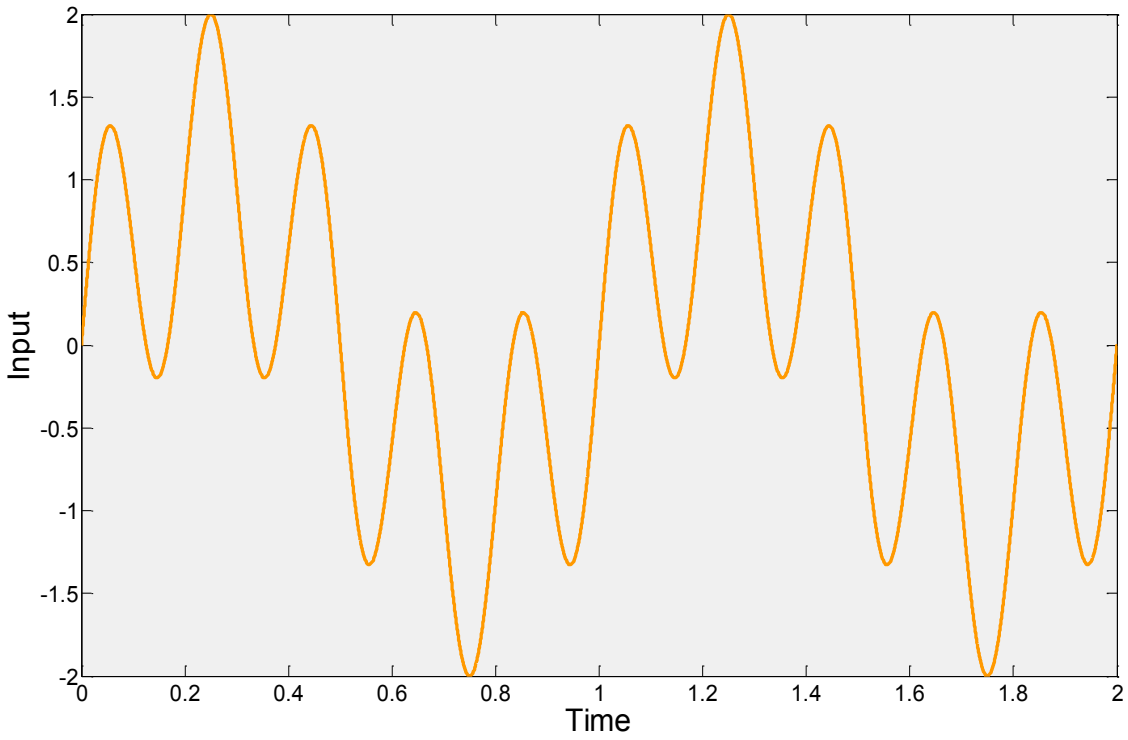

Figure 8. A nominal input vibration signal for $n = 5$ and $\omega = 2\pi$. This shows the input signal repeating every $\frac{2\pi}{\omega}$ or 1 second.

$$T = \frac{2\pi}{\omega} * 5$$

That is, the period of the total signal is five times larger than the period of the slower sinusoid $\frac{2\pi}{\omega}$. An example of this input is shown in Figure 9.

For $n = 2.3$ κ must be 10 for the product $n * \kappa$ to be an integer.

$$T = \frac{2\pi}{\omega} * 10$$

Indicating that the period of the signal $\sin(\omega t) + \sin(2.3\omega t)$ is 10 times larger than the period of $\sin(\omega t)$. This input is shown in Figure 10.

By substituting these expressions for the period of the input vibration into equation

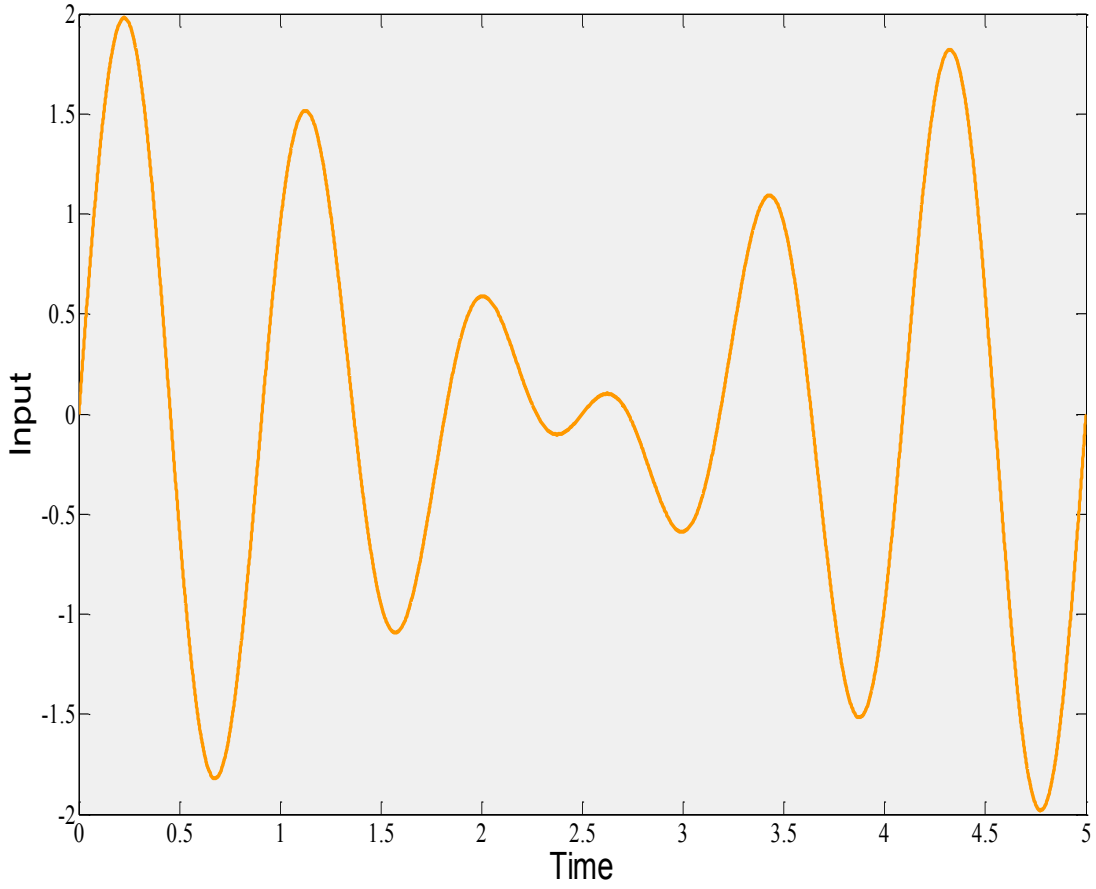

Figure 9. The input signal for $n = 1.2$ and $\omega = 2\pi$ plotted over one period of the entire input signal.

46, the net energy on the system from the time dependent component is shown to be:

$$E_{TD}\left(\frac{2\pi}{\omega}\kappa\right) = \frac{A^2m^3\begin{pmatrix}1-(-2+n)n-n(1+n)\mathrm{Cos}[2\kappa(-1+n)\pi]+\\(-1+n^2)\mathrm{Cos}[2\kappa n\pi]^2+(-1+n)n\mathrm{Cos}[2\kappa(1+n)\pi]\end{pmatrix}}{8b^2n^2} = 0 \qquad (49)$$

For $\kappa \in \mathbb{Z}^+$ and $n * \kappa \in \mathbb{Z}^+$, the condition where input has made a complete cycle, it can be shown that equation 49 reduces to zero. However, for $\kappa \notin \mathbb{Z}^+$ and $n * \kappa \in \mathbb{Z}^+$, that is not a multiple of the input period, the energy from the time dependent force remains

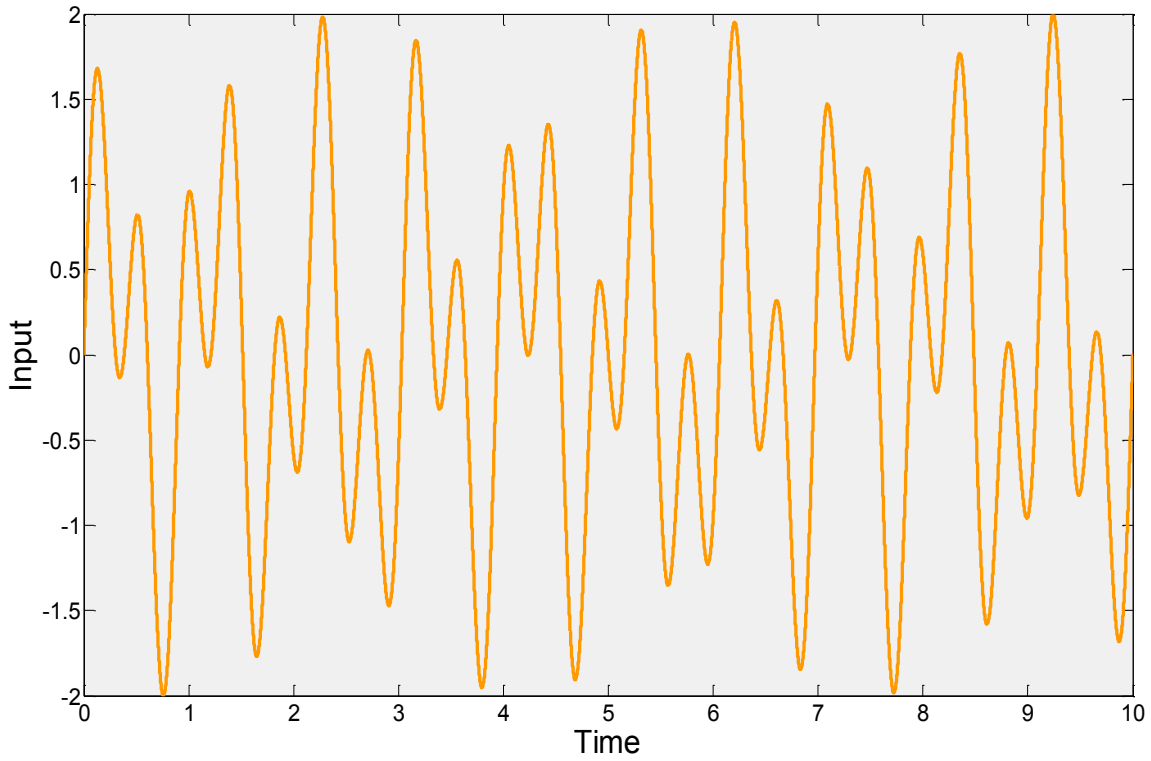

Figure 10. The input signal for $n = 2.3$ and $\omega = 2\pi$ plotted over one period of the entire input signal.

finite and bounded. Through these examples it has been shown that the time dependent portion of the transducer does not have a net effect on the energy balance for any input of the form shown in equation 38. In all cases, the time dependent component acts as a conservative element: transferring energy back and forth from the internal energy of the transducer to the kinetic energy of the proof mass. This relationship is characteristic of a spring, albeit with a more complex and time dependent constitutive law.

4.4 Energy Output Bound

The upper limit for energy output from the optimal transducer, with equation 38 as the input to the system, can be shown analytically. This can be accomplished in a similar

manner to the derivation of the average power output for the linear case shown in equation 33. Knowing that from the result of equation 42 the power output from the transducer is dissipated by the force of a linear viscous damper, the power dissipated through this element can be written as:

$$P = F * v = b_m x_2^{\star 2} \tag{50}$$

Here, $x_2^{\star}$ is the optimal velocity shown in equation 39. Integrating the instantaneous power output over time yields the total energy generated by the transducer. For simplicity and conciseness, the upper limit of the integral is taken to be $\mathbb{Z}$ times the period of the lower frequency sinusoid. The following analysis still holds true if the integral is evaluated for an arbitrary time interval.

$$E_n = \int_0^{\mathbb{Z}*\frac{2\pi}{\omega}} b_m x_2^{\star 2} dt \tag{51}$$

The integral is then evaluated in the general case for all $n \in (1, \infty)$ as well as the linear case at $n = 1$.

$$E_n = \frac{A^2\, m^2 \left(8\mathbb{Z}\pi - \frac{8\mathrm{Sin}[2n\mathbb{Z}\pi]}{n^2-1} - \frac{\mathrm{Sin}[4n\mathbb{Z}\pi]}{n}\right)}{16 b_m \omega} \tag{52}$$

$$E_1 = \frac{A^2 m^2 \pi \mathbb{Z}}{b_m \omega} \tag{53}$$

Looking at the ratio $\frac{E_n}{E_1}$ will yield the percentage of energy generated by the optimal transducer for any value of n as compared to the linear system with a single sinusoidal

vibration input at $n = 1$.

$$\frac{E_n}{E_1} = \frac{8\mathbb{Z}\pi - \frac{8\mathrm{Sin}[2n\mathbb{Z}\pi]}{n^2-1} - \frac{\mathrm{Sin}[4n\mathbb{Z}\pi]}{n}}{16\mathbb{Z}\pi} \tag{54}$$

It can be seen that for any fixed value of $n \neq 1$ the limit of equation 54 as $\mathbb{Z} \to \infty$ is,

$$\lim_{\mathbb{Z}\to\infty} \frac{8\mathbb{Z}\pi - \frac{8\mathrm{Sin}[2n\mathbb{Z}\pi]}{n^2-1} - \frac{\mathrm{Sin}[4n\mathbb{Z}\pi]}{n}}{16\mathbb{Z}\pi} \to \frac{1}{2} \tag{55}$$

That is to say, the maximum amount of energy that can be extracted from an input of two sinusoids separated in frequency by a factor n is half of the energy that can be produced by a linear system under a single sinusoid input of twice the amplitude. Another useful comparison of the energy output can be made with a linear system harvesting from only the lower of the two frequencies. In this case, the optimal transducer will produce twice the energy of the linear system.

The RMS power output for the optimal transducer can be found by first integrating equation 50 from zero to time t and then taking the limit as $t \to \infty$.

$$E_n = \int_0^{\mathrm{t}} b_m x_2^{\star 2} d\tau \; = \frac{A^2 m^2 \left(t + \frac{2n\mathrm{Cos}[nt\omega]\mathrm{Sin}[t\omega]}{\omega - n^2\omega} - \frac{\mathrm{Sin}[2t\omega] + \frac{\mathrm{Sin}[2nt\omega]}{n} - \frac{8\mathrm{Cos}[t\omega]\mathrm{Sin}[nt\omega]}{-1+n^2}}{4\omega} \right)}{4b_m} \tag{56}$$

The average power output can then be found through the following limit.

$$P_{RMS} = \lim_{t\to\infty} \frac{E_n}{t} = \frac{A^2 m^2}{4b_m} \tag{57}$$

Expressing in terms of the damping ratio:

$$P_{RMS} = \frac{A^2 m}{8\omega\zeta_m} \tag{58}$$

In comparison to the RMS power output of the linear system with matched mechanical and electrical impedance, as seen in equation 59, the power output of this system is twice the magnitude when expressed with the damping ratio.

$$P_{RMS} = \frac{A^2 m}{16\omega\zeta_m} \tag{59}$$

Here, the critical damping ratio ζ_m corresponds to the damping from the parasitic viscous mechanical damping and is defined as $\zeta_m = \frac{b_m}{2m\omega}$ for both equation 55 and 56.To verify these results a numeric study was performed. This study was performed using Matlab's ODE45 function. The energy output was measured after the system achieved steady state, in order to avoid transients affecting the solution. The results of this study confirm the analytical derivations above. An output of this study can be seen in Figure 11.

It can be seen that from the linear power equation that the power output from the system is proportional to the amplitude squared over ω, that is, $\propto \frac{A^2}{\omega}$ [2]. In the case of $n = 1$, $P \propto \frac{(A+A)^2}{\omega} = \frac{4A^2}{\omega}$. However, this simple substitution is only valid for the special case when $n = 1$. For a small perturbation of the upper sinusoid, $n = 1 + \delta$, the power output is $P \propto \frac{A^2}{\omega} + \frac{A^2}{\omega(1+\delta)}$. Where for a sufficiently small δ, $P \propto \frac{2A^2}{\omega}$. This power output for the slightly perturbed case is half of the power output of the case when $n = 1$.

As n grows larger the power output becomes $P \propto \frac{A^2}{\omega} + \frac{A^2}{n\omega}$. It can be seen that for

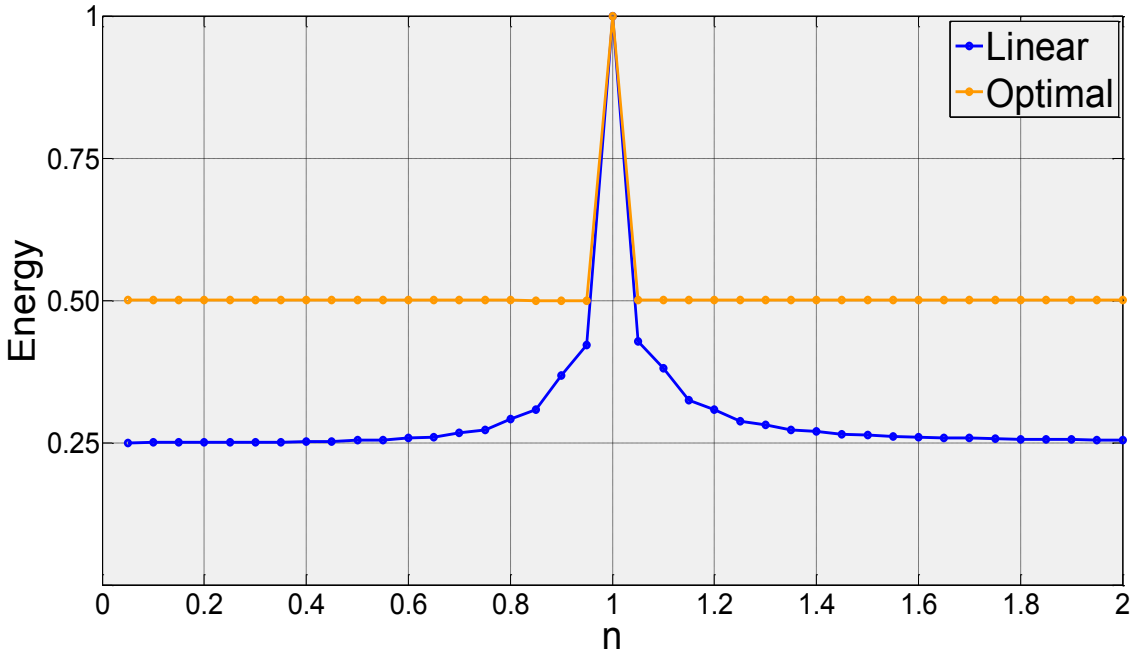

Figure 11. Numeric simulations of the energy output of the optimal transducer as compared to a linear harvester. The energy production has been normalized by the energy output of both systems at $n = 1$.

large values of n, $P \propto \frac{A^2}{\omega}$, which is a quarter of the power output seen in the case when $n = 1$.

4.5 Realizable Solutions

While in general the optimal solution is not realizable with a simple passive system, the results of this framework can be used as a guide to find a suboptimal passive solution. This ability is especially relevant in the cases when $n = 2$ and $n = 3$. The optimal restoring forces as a function of the relative displacement are shown in Figure 12 and 13. As can be seen, a single optimal solution exists for all negative values of the relative displacement. For positive values, two solutions exist. If an intermediate value between the two solutions is used then this optimal solution could be approximated as a single sided softening spring.

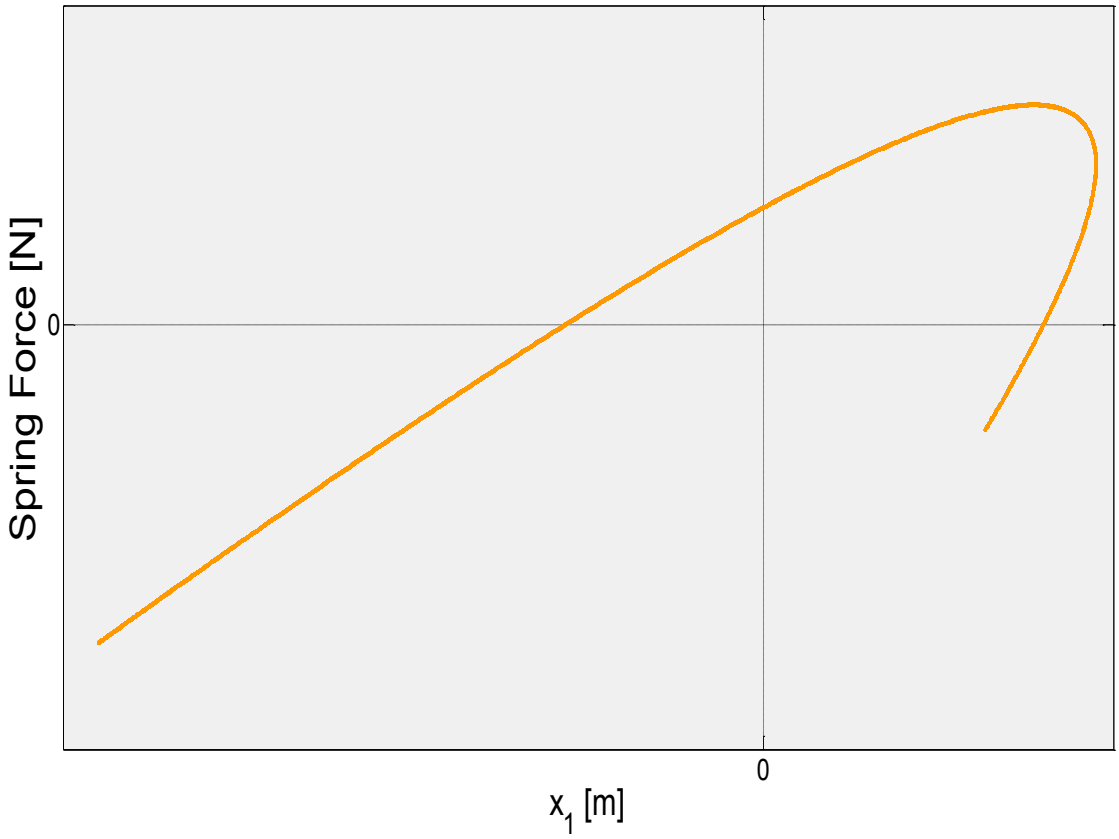

Figure 12. The restoring force as a function of the relative displacement x_1 for an input forcing function with $n = 2$.

The second example is shown in Figure 13. For this input, $n = 3$, the optimal restoring force is a single value as a function of the displacement. The restoring force is an extremely bistable function, a function that cannot be closely approximated by a bistable Duffing oscillator.

4.6 Conclusion

The result of this analysis shows that for an unconstrained transducer design, one that is inherently time dependent, the energy output of the system is independent of the separation of the two frequency components of the input. However, the RMS power output

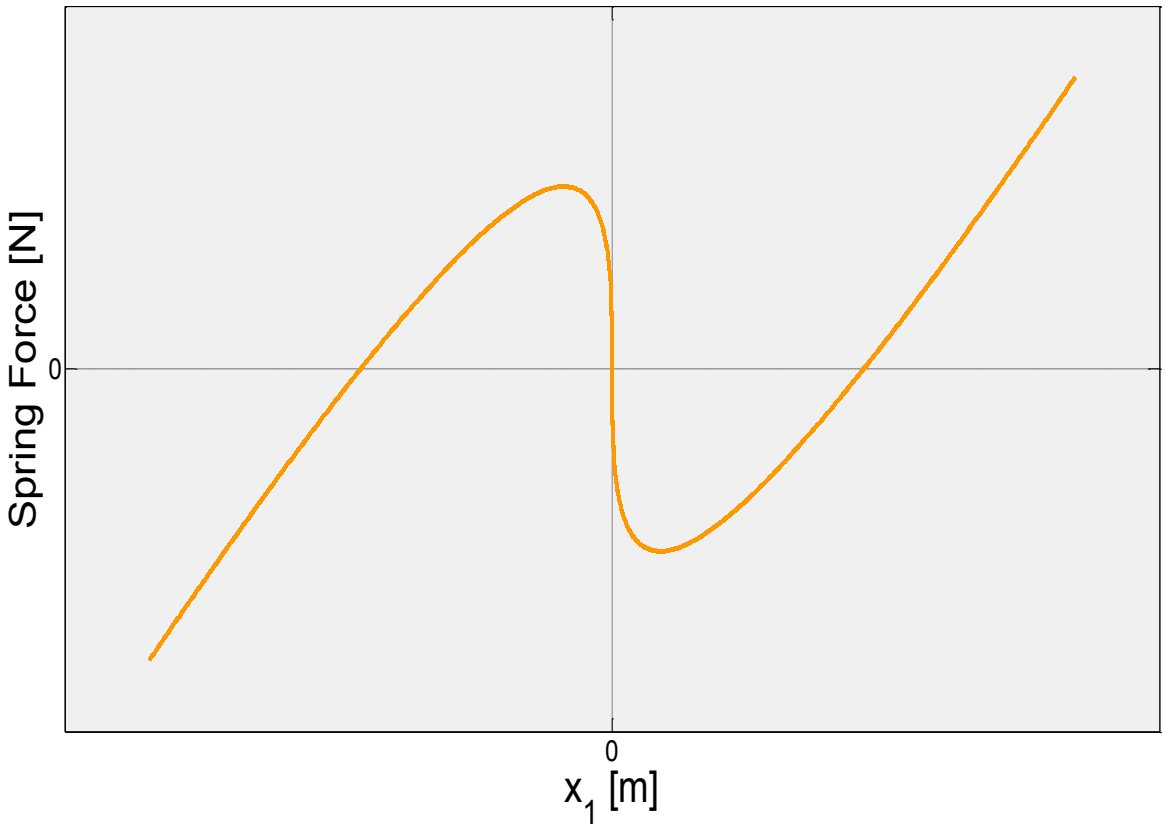

Figure 13. The restoring force as a function of the relative displacement x_1 for an input forcing function with $n = 3$.

from both input types, single and double sinusoid, are inversely related to the frequency of the lower sinusoid. An interesting conclusion from this analysis is that the maximum energy output is only a function of the lower of the two frequencies and completely independent of the separation between the two frequency components. Also, a linear harvester cannot successfully harvest energy from two inputs that are similar in frequency. The superposition of the two signals will greatly degrade each other lowering the energy output to at most half of the original combined signal.

CHAPTER 5[2]

THIRD APPLICATION – SWEPT SINUSOID INPUT

5.1 Introduction

Another common vibration input is one of a single sinusoid with a time dependent frequency. A common occurrence of this input type is found in a variety of transportation applications. These applications range from the quickly varying rotational speed of an automobile tire, as experienced by a tire pressure monitor (see Figure 14), to the slow changing excitation experienced by trains. Machinery with an unbalanced mass, whose rotational speed is time dependent, also experience this type of excitation such as that found in many industrial and manufacturing applications. Another occurrence of this input is in structural health monitoring. In this application the fundamental frequency of the structure changes very slowly with ambient conditions such as temperature.

The derivation of the optimal transducer for a single sinusoid is expressed in equation 29. This relationship proves that for a single stationary sinusoid vibration input the optimal transducer is a linear spring with matched resonance, and a linear viscous damper, with matched impedance to the mechanical damping. From this knowledge we can expect that for an input with changing frequency the optimal transducer should be a

[2] Portions of this chapter are forthcoming in, Heit, J., and Roundy, S., "A Mathematical Framework to Find the Upper Bound On Power Output as a Function of Input Vibration Parameters," (In Preparation)

Figure 14. The location of the tire pressure monitor sensor on consumer vehicles. All light vehicles in the United States manufactured after 2007 must be equipped with a TPMS system.

linear time dependent spring, resonant with the input frequency for all time, and a matched linear viscous damper.

The frequency of a sinusoid that varies linearly with time can be expressed as

$$f(t) = f_0 + f_r t \tag{60}$$

where $f(t)$ is the time dependent frequency, f_0 is the initial frequency of the sweep, and f_r is the rate at which the frequency changes with time.

Letting $\theta' = 2\pi f(t) = 2\pi(f_0 + f_r t)$ and integrating for θ from zero to some time t yields:

$$\theta = 2\pi \int_0^t (f_0 + f_r \tau)\, d\tau \tag{61}$$

$$\theta = 2\pi \left(f_0 t + \frac{1}{2} f_r t^2 \right) \tag{62}$$

Leaving the total time varying sinusoid input to be modeled by:

$$F(t) = A\ m\ sin(\theta) \tag{63}$$

$$F(t) = A\ m\ Sin\left[2\pi \left(f_0 + \frac{1}{2} f_r t \right) t \right] \tag{64}$$

5.2 Critical Velocity, Position, and Transducer Paths

Using the relationship from equation 13, corresponding to the maximum power output, the optimal velocity path as a function of the vibration input is described by:

$$x_2^\star = \frac{A\ m}{2b_m} \mathrm{Sin}\left[2\pi \left(\mathrm{f}_0 + \frac{1}{2} f_r t \right) t \right] \tag{65}$$

Equation 3 can be used to find the relationship for the optimal transducer force and is shown in equation 66. However, in this case equation 2 cannot be used to solve for the optimal position path of the proof mass, x_1, as an analytical solution to the integral of $x_2^\star$ can only be expressed through the use of Fresnel integrals. This relationship does not allow for a direct substitution of a function of x_1 for the optimal transducer force.

$$\begin{aligned} F_T^\star = {} & \frac{A\ m}{2} \mathrm{Sin}\left[2\pi \left(\mathrm{f}_0 + \frac{1}{2} f_r t \right) t \right] \\ & - \frac{\pi\ A\ m^2}{b_m} (f_0 + f_r t) \mathrm{Cos}\left[2\pi \left(\mathrm{f}_0 + \frac{1}{2} f_r t \right) t \right] \end{aligned} \tag{66}$$

The same substitution, as for the single and double sinusoid, can be made for the first term of equation 66 by a linear viscous damper model with matched impedance to the mechanical damping:

$$F_T^\star = b_m x_2 + TD \tag{67}$$

Here, TD is again the time dependent portion of the transducer force that cannot be substituted directly by the states of the system.

$$TD = -\frac{\pi A m^2}{b_m}(f_0 + f_r t)\mathrm{Cos}\left[2\pi\left(\mathrm{f}_0 + \frac{1}{2}f_r t\right)t\right] \tag{68}$$

5.3 Assumed Optimal Transducer

With the single sinusoid case in mind the mathematical framework can be used to check the validity of the assumed optimal transducer. Specifically, the optimal transducer is assumed to be a linear spring with a time dependent stiffness coefficient that is resonant with the input frequency at all times. Since the viscous damping which represents energy generation is already expressed in equation 67, the missing component of the assumed transducer is this time-varying spring component. It is assumed that the time dependent portion of the transducer force is this time dependent spring. Mathematically this assumption is expressed as:

$$TD = k(t)x_1 = \omega(t)^2 m\, x_1 = \left(2\pi(f_0 + f_r t)\right)^2 m\, x_1 \tag{69}$$

This relationship can be used to find an expression for x_1 that can subsequently be differentiated for x_2. To validate the accuracy of our assumption in equation 69, x_2 from

the assumed optimal transducer architecture will be compared to $x_2^\star$ in equation 65.

Substituting equation 68 into equation 69 and solving for x_1 yields:

$$x_1 = -\frac{A\,m}{4\pi b_m(f_0 + f_r t)}\,\mathrm{Cos}\left[2\pi\left(\mathrm{f}_0 + \frac{1}{2}f_r t\right)t\right] \tag{70}$$

By differentiation the velocity path of the assumed optimal transducer x_2 is found to be:

$$\begin{aligned} x_2 = {} & \frac{A\,m\,f_r}{4\pi b_m(f_0 + f_r t)^2}\,\mathrm{Cos}\left[2\pi\left(\mathrm{f}_0 + \frac{1}{2}f_r t\right)t\right] \\ & + \frac{A\,m}{2b_m}\,\mathrm{Sin}\left[2\pi\left(\mathrm{f}_0 + \frac{1}{2}f_r t\right)t\right] \end{aligned} \tag{71}$$

Examining the two components of equation 71 we can see that the second term is identical to the expression of $x_2^\star$ in equation 65. The first term of the expression is a transient sinusoid with decaying amplitude. An example comparison between x_2 and $x_2^\star$ is shown in Figure 15 with unitary values of the parameters and a relatively large value for f_r.

The transient component that causes the incongruity between x_2 and $x_2^\star$ is only appreciable for large values of f_r over small time scales relative to the initial period $\frac{1}{f_0}$. In application, the value of f_r will generally be fairly small as any implementation will require an input of energy to adjust the resonance frequency of the system.

Through this example we have shown that the mathematical framework can be used to validate an assumed optimal architecture. This framework can be used as a basis of comparison between transducer architectures and as a mark of feasibility for implementing a vibration energy harvester for a given vibration input and power requirement.

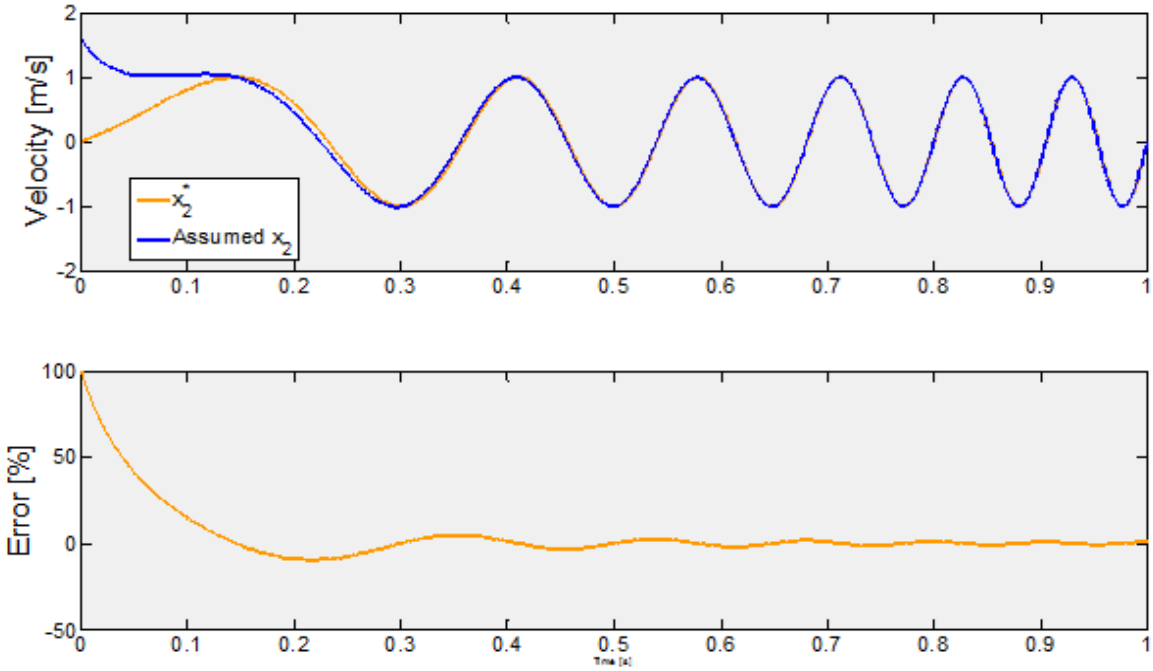

Figure 15. A comparison between the optimal and assumed solutions. (Top) x_2 and $x_2^\star$ versus time for $A = 1, m = 1, b_m = 1, f_0 = 1, f_r = 10$. (Bottom) The percentage error between the two signals in time. The error quickly decays to zero as the amplitude of the transient decays.

5.4 Energy Output Bound

The upper limit for the energy output of the optimal transducer for a swept sinusoidal input can be found in the same manner as the double sinusoid. By looking at the energy balance in equation 4 the energy generated can be described as:

$$\begin{aligned} & E_{gen} \\ &= \int_0^t \left[F(t)x_2^\star - b_m x_2^{\star 2}\right] d\tau \\ &= \frac{A^2 m^2 \left(2\sqrt{\mathrm{f_r}}t + \mathrm{Cos}\left[\frac{2\mathrm{f_0}^2\pi}{\mathrm{f_r}}\right]\left(\mathrm{C}\left[\frac{2\mathrm{f_0}}{\sqrt{f_r}}\right] - \mathrm{C}\left[\frac{2(\mathrm{f_0}+\mathrm{f_r}t)}{\sqrt{\mathrm{f_r}}}\right]\right) + \left(\mathrm{S}\left[\frac{2\mathrm{f_0}}{\sqrt{f_r}}\right] - \mathrm{S}\left[\frac{2(\mathrm{f_0}+\mathrm{f_r}t)}{\sqrt{\mathrm{f_r}}}\right]\right)\mathrm{Sin}\left[\frac{2\mathrm{f_0}^2\pi}{\mathrm{f_r}}\right]\right)}{16 b_m \sqrt{\mathrm{f_r}}} \end{aligned} \quad (72)$$

where $C[\,]\ and\ S[\,]$ represent the Fresnel integrals; defined as $C[v] = \int_0^v Cos\left[\frac{\pi t^2}{2}\right] dt$ and $S[v] = \int_0^v Sin\left[\frac{\pi t^2}{2}\right] dt$, respectively, over an arbitrary time interval v. Noting the

boundedness of $C[\,]$ and $S[\,]$, as shown in Figure 16, an approximation of the energy generated over large periods of time can be expressed as:

$$E_{gen} \cong \frac{A^2 m^2}{8 b_m} t \tag{73}$$

This approximation converges more quickly in time for large values of the ratio $\frac{2f_0}{\sqrt{f_r}}$. That is to say this approximation is more accurate for slow changes in the input frequency relative to the starting frequency. For relatively large time intervals the bounded components of the energy are insignificant compared to the time dependent components.

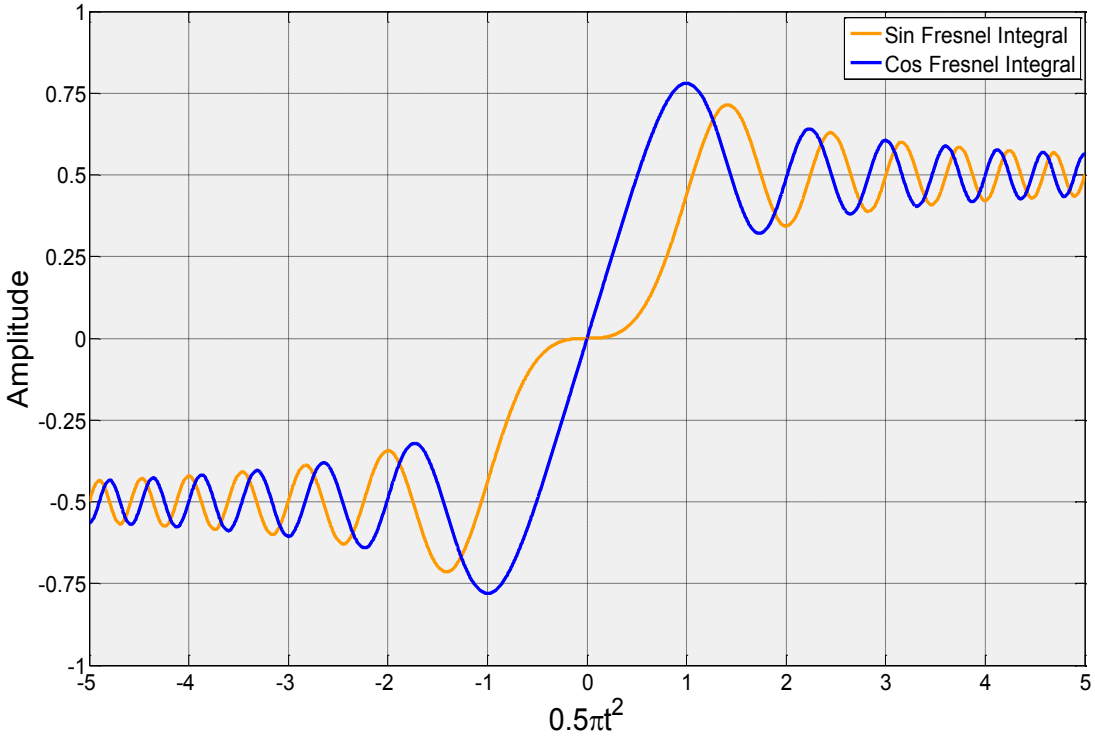

Figure 16. Plot of the sine and cosine components of the Fresnel integral $C[v] = \int_0^v Cos\left[\frac{\pi t^2}{2}\right] dt$ and $S[v] = \int_0^v Sin\left[\frac{\pi t^2}{2}\right] dt$. Both of these two integrals go to $\pm\frac{1}{2}$ as $t \to \pm\infty$.

The average power output can be expressed as:

$$P_{RMS} = \frac{\mathrm{dE_{gen}}}{\mathrm{dt}} = \frac{A^2 m^2}{8 b_m} \tag{74}$$

This power output for this time dependent input is identical to the power output found for a linear system, harvesting from a single sinusoid when expressed using the damping coefficient rather than the damping ratio. When expressed as a function of the linear viscous damping coefficient the power becomes a function of the time dependent input frequency.

5.5 Energy Balance with Tuning Penalty

The introduction of a tunable element will require energy from the system in order to monitor and adjust the resonance frequency of the structure. This will require the energy balance of the system to be reexamined with an additional energy consumption term. The energy consumption of the actuator will have two main components. The system will monitor the input frequency in order to correctly adjust the system and require energy for the actuation. By assuming an average power consumption $P_{monitor}$, the average energy output can be expressed as $E_{monitor} = \int P_{monitor}\, dt$. For the actuation of the system, a gain parameter, of the form $G = \frac{Change\ in\ frequency\ [\Delta\omega]}{Energy\ required\ [J]}$, is assumed to characterize the energy required for tuning the structure. This gives the time dependent energy required to continuously tune the system to be resonant with the input as:

$$E_{tuning} = \frac{1}{G}|\Delta\omega| = \frac{|2\pi f_r t|}{G} \tag{75}$$

The energy balance of the system is written as:

$$E_{in} = E_{out} + E_{gen} + E_{tuning} + E_{monitor} \tag{76}$$

Here, $E_{in}\ and\ E_{out}$ are the same as in equations 5 and 6. Substituting these values into the energy balance we find:

$$E_{gen} = \left[\frac{A^2 m^2}{8b_m} - \frac{2\pi f_r}{G} - P_{monitor}\right] t \tag{77}$$

For the system to be net energy positive, producing more energy than it consumes for monitoring and actuating, the expression for the RMS power output must be positive.

$$P_{RMS} = \frac{A^2 m^2}{8b_m} - \frac{2\pi f_r}{G} - P_{monitor} \tag{78}$$

5.6 Conclusion

This power output can be used to determine the feasibility of using a tunable system for harvesting energy from a swept sinusoidal vibration input. The feasibility is a function of the proof mass which may be limited in the design by the density of available materials and volume constraints, the amplitude of the acceleration vibration input, and the mechanical damping, which is limited by the manufacturing process as well as maximum displacement allowed by the proof mass. The tunable portion of the harvester also dictates the feasibility based on the average power consumption to monitor the system and the energy required to tune the system to the changing input frequency f_r.

CHAPTER 6

TUNABLE LINEAR HARVESTERS

6.1 Introduction

The near optimal transducer, as shown in the previous section, through equations 67 and 68, is in general a realizable system. Recently, considerable effort has been put into creating a device with adjustable stiffness for matching the frequency of the input vibration. Linear tunable harvesters, as they are known, can change their resonance frequency while remaining linear. This is accomplished by altering one or both of the parameters in equation 79 for the natural frequency of a single degree of freedom resonant harvester.

$$f_n = \frac{1}{2\pi}\sqrt{\frac{k_{eff}}{J_{eff}}} \tag{79}$$

Here, k_{eff} and J_{eff} are the effective stiffness and inertia, respectively. For practical reasons, typically the effective stiffness, rather than the effective mass, is the control parameter of choice for these tunable devices due to physical limitations. Many novel and creative methods have been used to alter the effective stiffness of vibration energy harvesters.

6.2 Previous Work on Tunable Harvesters

Mukherjee *et al*. as well as Ivo *et al.* proposed using magnets to create an axial tensile force between the proof mass and the base [17] [18]. This was accomplished through the use of two magnets, one located at the proof mass and the other on the base. The resonance frequency of the system is adjusted by changing the distance between these two magnets. A diagram of this system design is shown in Figure 17. This design has the benefits of being simple, (only one degree of freedom to actuate) compact, and has a relatively high tuning gain. However, the effective actuation range is small since the magnetic force falls off quickly with actuated displacement. Another drawback of this design is the introduction of a nonlinear restoring force to the proof mass by the magnetic forces. The introduction of this nonlinearity creates a deviation from the optimal transducer, shown in equation 62.

Challa *et al.* proposed the addition of magnetic springs to a piezoelectric cantilever beam in order to modify the effective stiffness [19]. The diagram of this system can be seen in Figure 18. By adjusting the relative displacements between the magnets d_a and d_r, the resonance frequency of the system can be attuned to higher and lower frequencies. This system has the benefit of a high sensitivity and large actuation range. However, the system's stiffness is nonlinear. This deviation in stiffness linearity adversely affects the power output for a swept sinusoid when compared to a continuously tuned linear system.

Peters *et al*. built and tested a novel device shown in Figure 19 [20]. This device was able to alter the geometry and mechanical advantage of three parallel cantilever springs in order to change the stiffness of the structure. This device worked on the principle of applying an electric potential across the faces of two piezoelectric beams

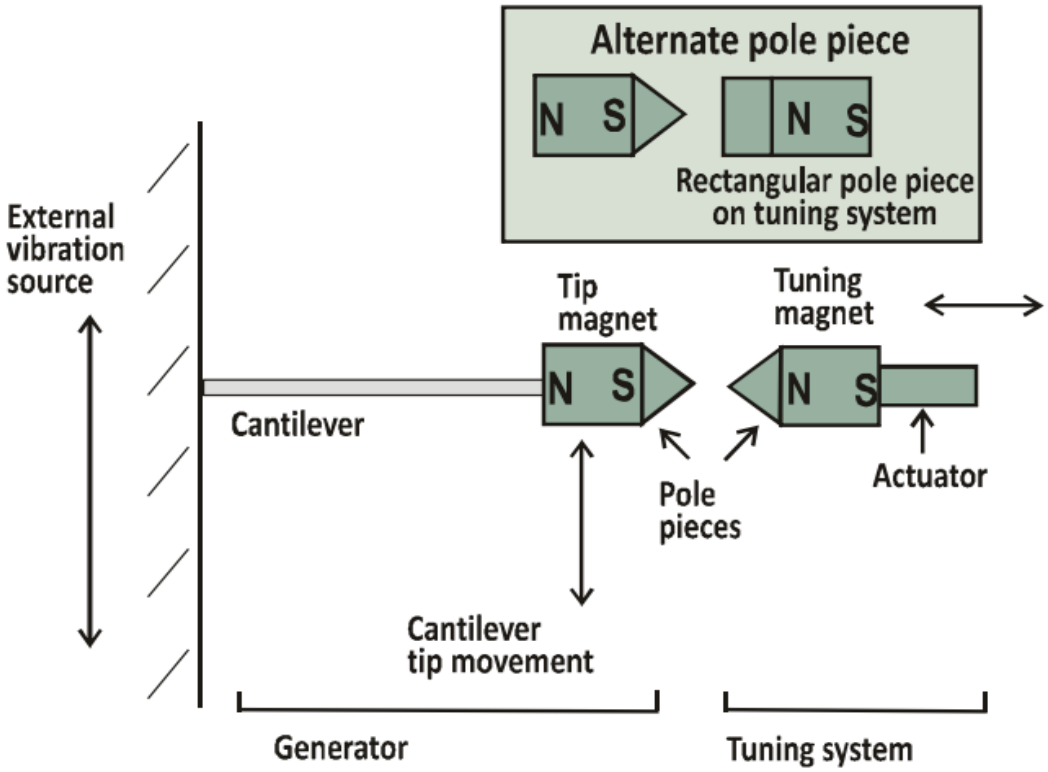

Figure 17. Diagram of the tunable harvester modified from, A. Mukherjee, P. Mitcheson, E. Yeatman, D. Zhu and S. Beeby, "Magnetic Potential Well Tuning of Resonant Cantilever Energy Harvester," PowerMEMS, 2012. The frequency of the device is tuned by adjusting the distance of the left most magnet. Changing this displacement alters the axial force in the cantilever beam, changing the effective stiffness of the structure.

mounted perpendicular to the free and fixed ends of three cantilever beams used for power generation, labeled as hinges in Figure 19. When no voltage is applied to the piezoelectric actuators, the system is contained to a plane when not excited by an input vibration. However, when a voltage is applied to the piezoelectric actuators, the actuators bend out of plane causing the outer two hinges to elevate a small distance above the center hinge. This change in geometry causes an increase in the effective stiffness. Drawbacks of this system include large voltage requirements that may not be available in application, low tuning range and sensitivity. In addition, this system requires continuous energy draw to maintain the new tuned state.

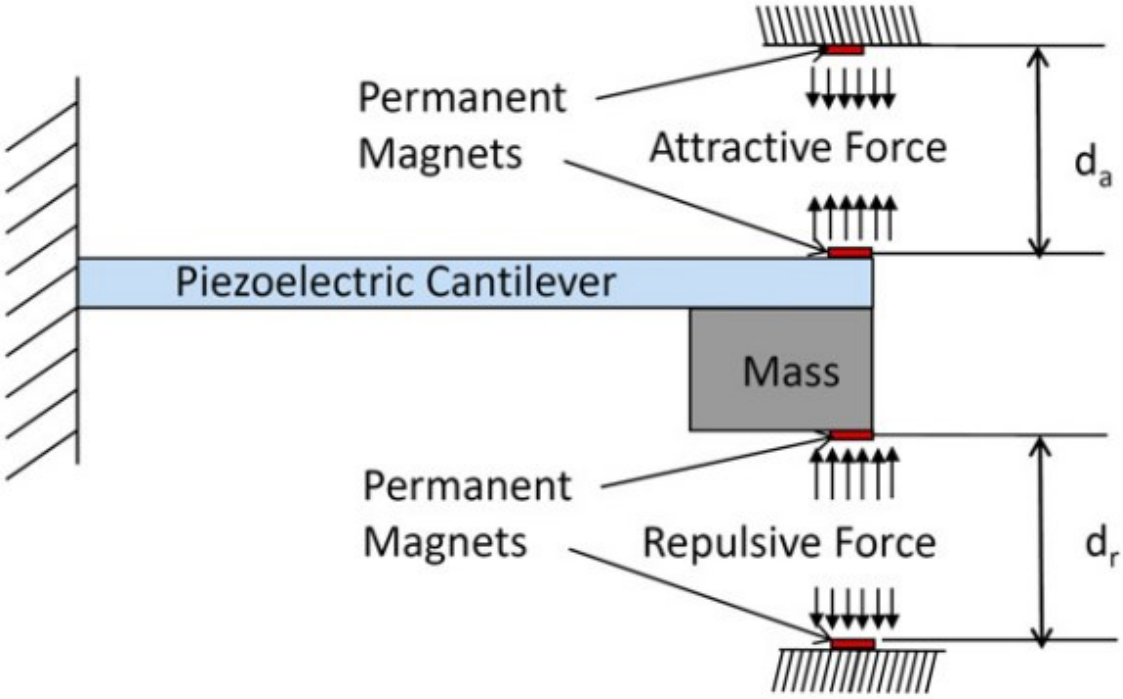

Figure 18. This diagram, modified from, V. R. Challa, M. G. Prasad, Y. Shi and F. T. Fisher, "A Vibration Energy Harvesting Device with Bidirectional Resonance Frequancy Tunability," Smart Materials and Structures, vol. 17, pp. 015035, 2008 works by altering the relative displacements d_a and d_r. Through this change, the effective stiffness of the structure can be altered.

As a final example, Shyh-Chin Huang and Kao-An Lin at Ming Chi University of Technology created a device that exploits the cubic relationship between the stiffness of a cantilever beam and its length [21]. By moving the location at which the beam is supported, the effective length of the cantilever beam is shortened and the stiffness is greatly increased. A diagram of this type of system is shown in Figure 20. This device has the advantage of a large tunable range while remaining linear. This system requires a large actuation distance giving the overall system low sensitivity. The use of piezoelectric materials located at the tip of the cantilever beam also has the constraint of being placed in a low strain area of the beam, leading to lower voltages and damping coefficients. Additionally, systems of this design have an inherently low mechanical quality factor.

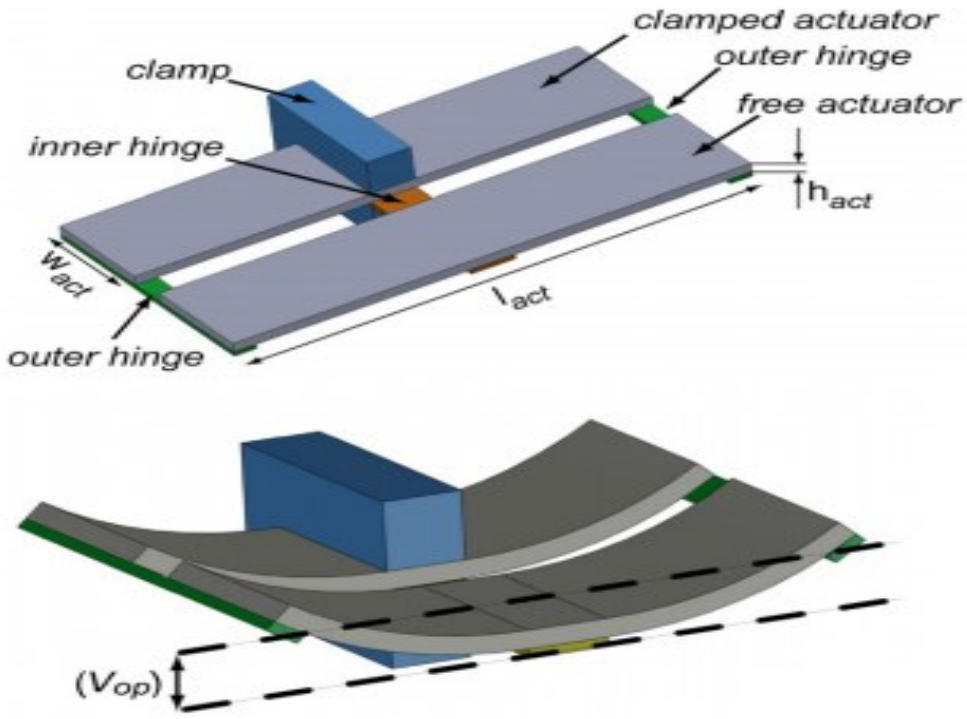

Figure 19. A modified diagram of the device built and tested by C. Peters, "A Closed-Loop Wide-Range Tunable Mechanical Resonator for Energy Harvesting Systems, " Journal of Micromechanics and Microengineering, vol. 19, pp. 094004, 2009. The device shown here is only the mass-spring component of the harvester. By applying a voltage to piezoelectric actuators, the beams bend upwards, increasing the stiffness of the structure.

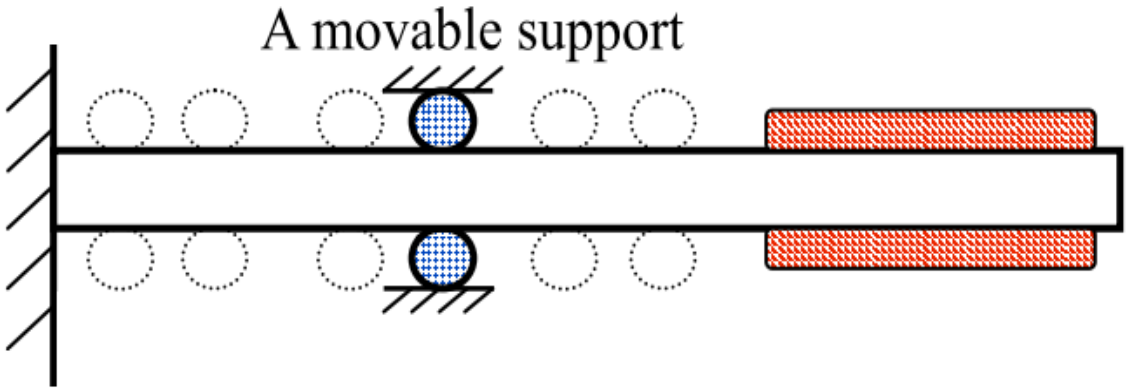

Figure 20. The modified diagram of the tunable linear energy harvester by L. S.-C. Huang and Kao-An, "A Novel Design of a Map-Tuning Piezoelectric Vibration Energy Harvester," Smart Materials and Structures, vol. 21, pp. 085014, 2012. The stiffness of the structure is adjusted by changing the location of the base of the cantilever beam.

CHAPTER 7[3]

WISHBONE DESIGN

7.1 Introduction

A tunable vibration energy harvester was designed, constructed, and characterized based on the principles from equations 66 – 69. This harvester was designed to avoid the complications presented in previous work. These complications include the use of high voltages that are often unavailable to the device in practice, a low tuning gain that requires large displacements to tune the resonance frequency of the structure, and continuous power consumption to maintain the tuned state. The unintentional introduction of nonlinearities into the system will cause a significant deviation from the optimal transducer, resulting in a lower energy output.

An abstract of this design in various state is shown in Figure 21.The complete structure, as shown in Figure 22 is comprised of three main components: the tunable spring structure, the control structure, and the proof mass. The novelty of this vibration energy harvester is the spring and control structure. The springs, dubbed wishbone springs or wishbones, each consist of two cantilever beams held apart by the proof mass at the free end. The fixed end of the bottom beam is held to the base of the structure and the top

[3] Portions of this chapter are forthcoming in, Heit, J., and Roundy, S., "A Compact Vibration Harvester, Tunable Over a Wide Frequency Range, Using Minimal Actuation," Energy Harvesting Journal, (In Preparation)

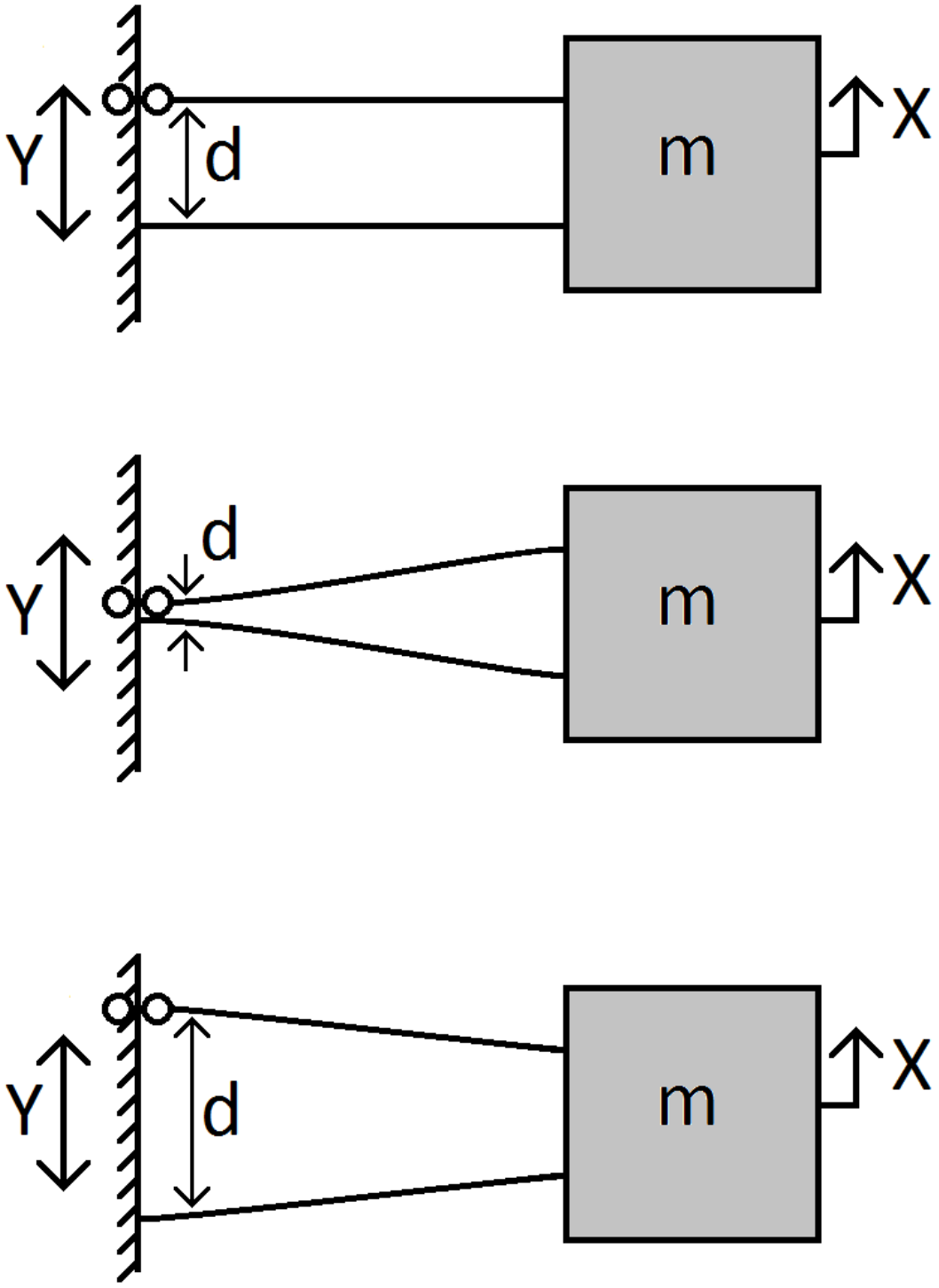

Figure 21. Diagram showing the actuation concept of the wishbone spring. The base separation d is adjusted by taking the two cantilever beams from parallel to an acute angle, decreasing the mechanical advantage, or to an obtuse angle, increasing the mechanical advantage of the spring on the mass.

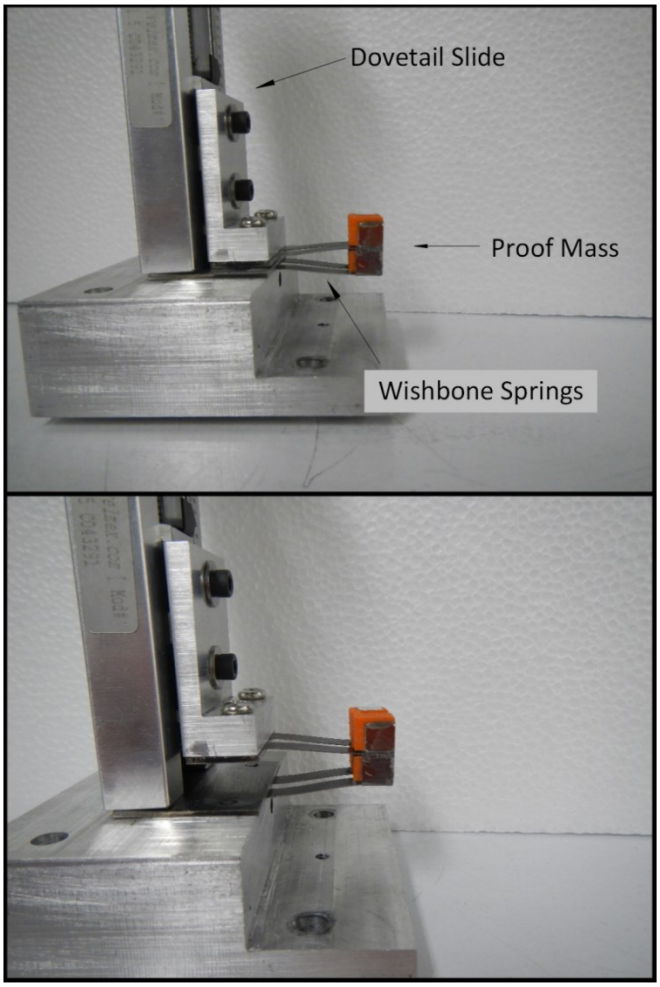

Figure 22. Photo of the prototype of the wishbone design, used to validate the practicality of creating a tunable linear harvester shown at the limits of the adjustment.

cantilever beam is mounted to a dovetail slide that can be actuated vertically. As can be seen in Figure 21and 22 the distance between the beams can be adjusted, changing the effective stiffness of the structure by altering the mechanical advantage and axially loading the beams. When implemented, two of these wishbone beams are used in series in order to hold the permanent magnets required for the electromagnetic generator portion of the transducer.

7.2 Prototype

For the construction of a prototype a precision dovetail slide was used for the control structure. This device actuates the base of the top beams. The dovetail slide gives an easy adjustment for the base separation distance in order to evaluate the effectiveness of this design. The cantilever beams used for the wishbone spring are constructed from 1090 spring steel. The proof mass is comprised of rare earth magnets that can be incorporated into an electromagnetic generator.

7.3 Mechanical Damping

The mechanical damping coefficient must be measured in order to match the electrical damping to the mechanical damping. For this system, the mechanical damping was found by examining the response of the proof mass to a slow swept sinusoid base excitation. The mechanical damping of the system was found through the relationship:

$$b_m = 2\zeta\omega_n m = \frac{\omega_n m}{Q} \tag{80}$$

where Q is defined through the relationship:

$$Q = \frac{f_n}{\Delta f} \tag{81}$$

Here, f_n is the resonance frequency and Δf is the half power bandwidth. This test was performed multiple times for interval values of the base separation d. From these relationships the quality factor of the system was found to be approximately constant at $Q \cong 40$.

With a proof mass of 8 grams, as was used in testing, the mechanical damping coefficient was found to be:

$$b_m = 1.57E^{-3} f_n = 1.57E^{-3}(f_0 + f_r t) \quad (82)$$

This information of the mechanical damping is crucial in the design of an optimal electric transducer for the system. As with a linear system, the power output of the swept sinusoid is maximized when the two damping ratios are equivalent, as can be seen in Figure 4. Unlike the constant sinusoid vibration input, the damping coefficient in equation 82, is time dependent through the changing resonance frequency of the system.

Depending on the magnitude of change in the input frequency f_r and the time interval that the harvester is collecting energy, the damping coefficient may need to be time dependent. This can be accomplished through a mechanism that offsets the coils in the magnetic field. If the change in the natural frequency is expected to be relatively small, the value of electrical damping can be constant and chosen such that the range in damping values is centered at the peak of Figure 4. In general, the design of energy harvesters are not extremely sensitive to the damping ratio. Often, in practice, the electrical damping coefficient is limited by physical constraints such as: magnetic field strength, number or coils in an electromagnetic generator, or the coupling coefficient of the piezoelectric material. Because of these limitations, the design objective of a vibration energy harvester is to minimize the mechanical damping and maximize electrical damping.

Figure 23 shows a photo of the test setup used for the dynamic testing. The device was attached to a shaker table controlled through Labview to simulate a base excitation. The response of the proof mass was then measured using the laser vibrometer.

Figure 23. Photo of the test setup. The shaker table provided the base excitation to the structure and the laser vibrometer measured the response of the proof mass.

7.4 Verifying Linearity of the Restoring Force

Fourier transforms of the swept sine data were used to find the resonance frequency of the system. This technique depends on the linearity of the restoring spring force. If the spring force is nonlinear, the amplitude of the input vibration as well as the direction of the sweep can greatly impact the measured resonance frequency. In addition, it has been shown that for nonlinear systems the net damping on the system can affect which solution the response manifests [10]. In order to determine the system's linearity two tests were performed. First, the direction of the sine sweep was reversed and the measured resonance frequency of the system's response was compared. These data are shown in Figure 24. Second, the restoring force of the spring was measured through a static deflection test. These test results are shown in Figure 25.

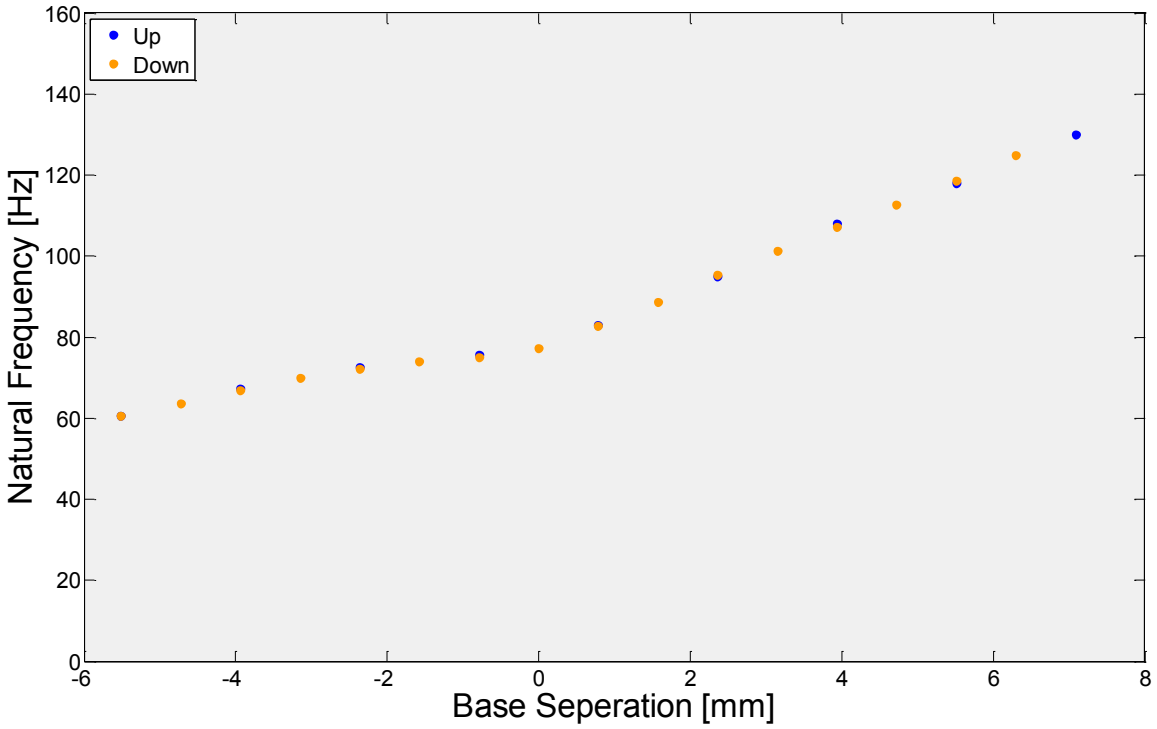

Figure 24. Resonance frequency as a function of the base separation for sinusoid sweeps in both directions. The small variation between the two values for a given base separation indicates the linearity of the system.

Through the derivative, the slope of the curves gives the stiffness parameter of the linear restoring force. This stiffness is shown in Figure 26 as a function of base separation. Assuming a simple 1 DOF model, as in equation 1, the resonance frequency of the system can then be calculated through equation 75. Using the proof mass of 8 grams that was used in the sinusoid sweeps, the natural frequency based on the static stiffness data can be calculated. Figure 27 shows the natural frequency of the system as measured by the sinusoid sweeps and calculated based on the measured static stiffness. Both methods for determining resonance, static deflection, and dynamics sweeps give extremely close results. These results give the device a tunable range from 60-130 Hz.

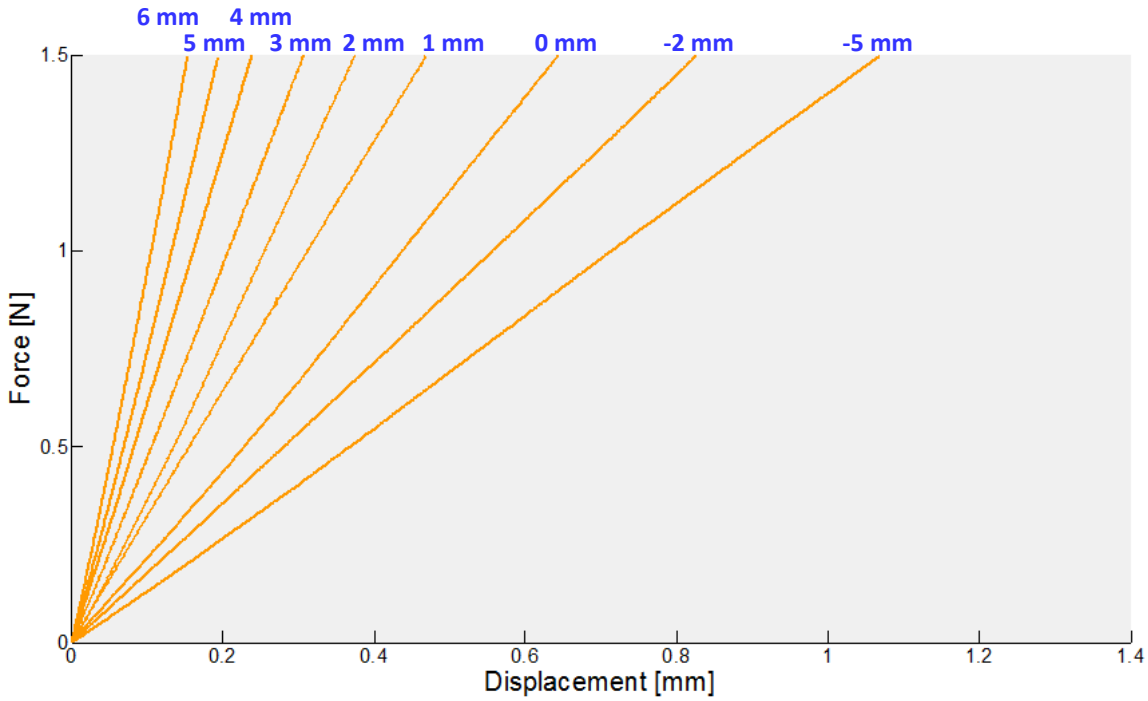

Figure 25. The static force versus deflection at incremental values of the base separation d.

7.5 Conclusions and Future Work

The device shown here has been based on the optimal transducer model for a linearly time varying sinusoid, as shown in equation 62. The optimal transducer must have a time dependent linear restoring force and an electrical transducer with matched impedance to the mechanical damping. As was shown through the resonance frequency from swept sin inputs, as well as static stiffness data, this device was shown to remain linear through the actuation range. The device was also able to remain resonant over a wide frequency range of the input vibration.

A comparison of tunable vibration harvesters is shown in Table 2. This table shows the actuation range in applicable units, the tuning range as a percentage of the mean, and tuning sensitivity. The tuning sensitivity is not directly comparable as some devices actuate based upon different principles, such as voltage or geometry. While this device does not

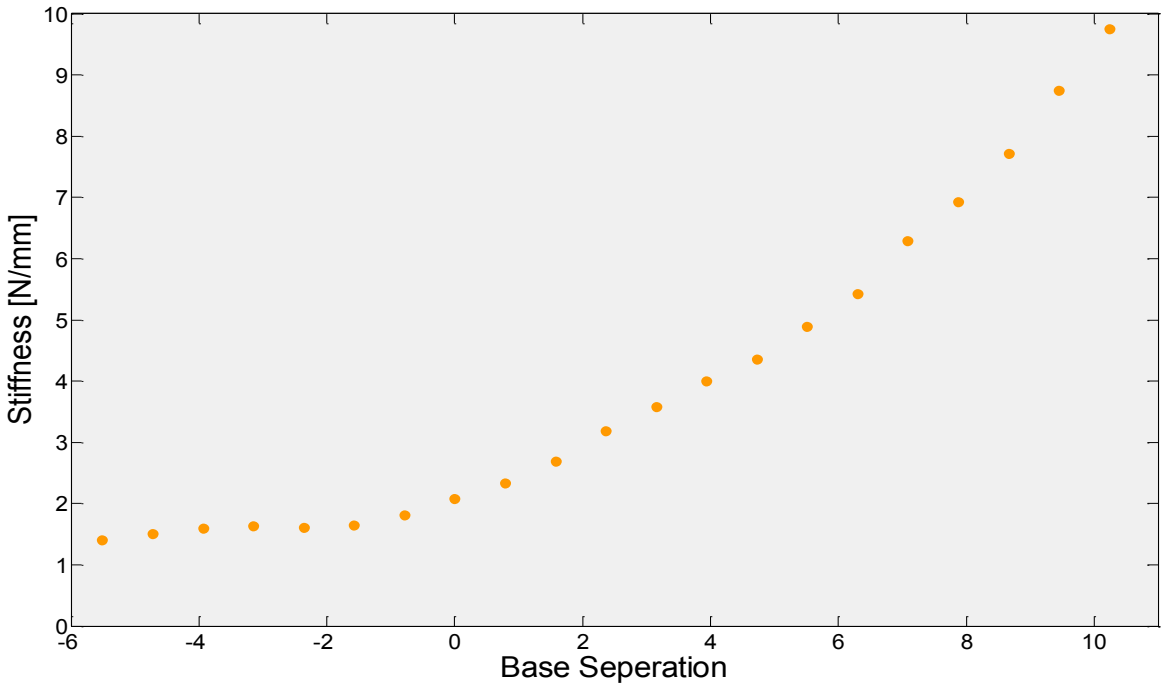

Figure 26. The linear stiffness coefficient as a function of base displacement d.

have the highest tuning sensitivity or actuation range, it does possess a good combination of each. As can be seen in Figure 27, the resonance frequency is more sensitive for positive values of the base separation. If the actuation range is restricted to positive values of the base separation, the tuning range and sensitivity are $\pm 24\%$ and $7.7 \frac{mm}{Hz}$, respectively.

Before a suitable device can be implemented the system must be scaled down to work with a wireless sensor network. This will require examining different types of actuators that consume small amounts of energy and do not consume power to remain in a tuned state. Equation 74 can be used to check the feasibility of implementing this tunable harvester for a given vibration input. The energy generated by this tunable device can then be compared to the energy generation for a well-designed passive vibration energy harvester.

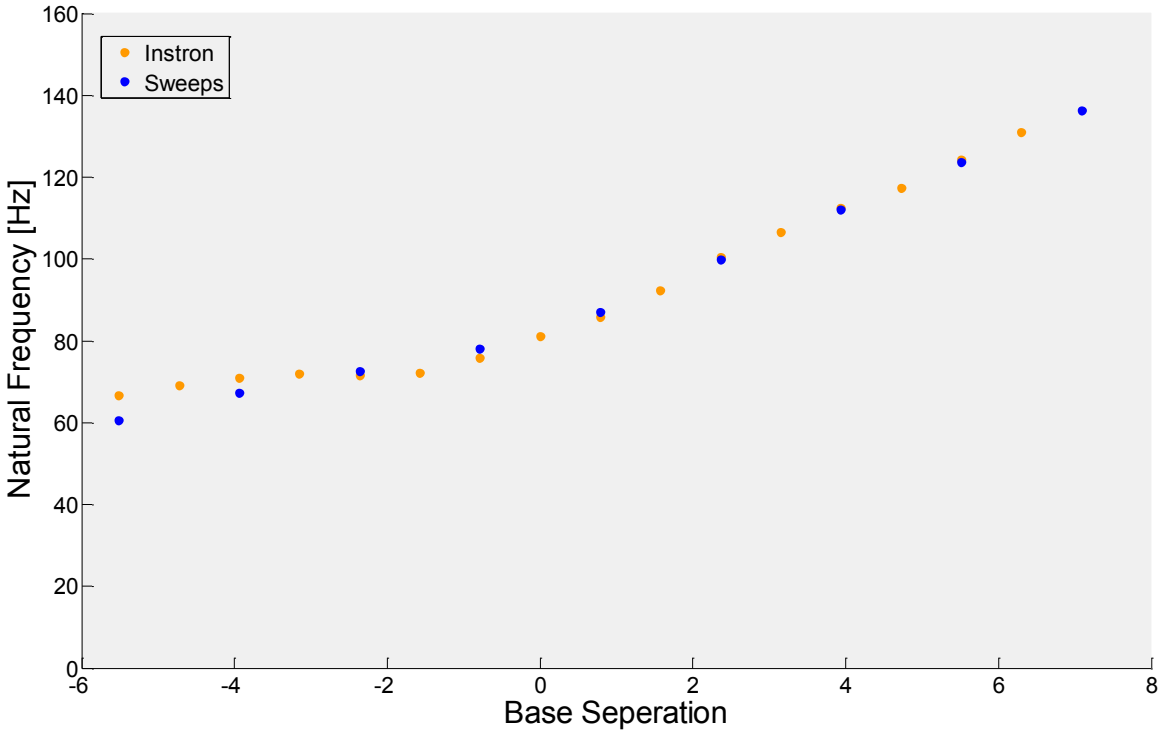

Figure 27. The natural frequency of the system as a function of the base separation. The orange points represent the resonance frequencies as calculated from the stiffness from the quasistatic Instron testing. The blue points are the measured natural frequency from the sin sweeps.

Table 2. Comparison of tunable energy harvester in recent published work. Note that the actuation range and sensitivity numbers are not nondimensionalized, so there is not a perfect comparison between devices.

Ref.	Author(s)	Actuation Range	Tuning Range	Tuning Sensitivity
[20]	Christian Peters et al.	10 V	±15%	2.3 Hz/V
[22]	C. Elchhorn et al.	70 V	±18%	0.9 Hz/V
[21]	Shyh-Chin Huang et al.	35 mm	±32%	2.3 Hz/mm
[18]	Ivo Ayala et al.	2 mm	±10%	7.0 Hz/mm
[14]	Mohamed Mansour et al.	54 mm	±58%	0.2 Hz/mm
[19]	Vinod Challa et al.	N/A	±19%	N/A
	This Work	12mm	±37%	5.8 Hz/mm

CHAPTER 8

CONCLUSION

This thesis has outlined the necessary mathematical framework to relate input vibration characteristics to the transducer force that maximizes energy generation of a vibration energy harvester. Through this framework the theoretical upper limit on the amount of energy harvested has been determined for a given vibration input. The relationship between the vibration input and energy generation limit defines the optimal transducer force. This relationship can be used as a guide to the design of a transducer for a given vibration input. Based on the relationship found between the vibration input of a swept sinusoid, a tunable vibration energy harvester was built and characterized to mimic the dynamics of the optimal transducer.

To develop the framework, a 1 DOF model was used consisting of a proof mass, parasitic mechanical loss, modeled by a linear viscous damper, and an unknown transducer force. An energy balance was used to define the functional of the energy generated by the system. Using the stationary condition of the Euler-Lagrange equations, the critical points of the energy output were found with respect to the velocity of the proof mass. Through the governing differential equations, the transducer force that will produce this velocity path of the proof mass was found as a function of the vibration input.

To validate the mathematics, first the framework was applied to an input of a single

sinusoid. The three solutions to the critical proof mass velocity paths yielded two minimums and a maximum for energy output. The first minimum solution corresponds to a system in resonance with no electrical energy transduction mechanism. The other minimum solution corresponds to the trivial solution with no relative displacement of the proof mass. Here, the transducer force is equal and opposite to the input. This can be visualized as a transducer that consists only of a single spring with infinite stiffness. The maximum solution, corresponding to the optimal energy output, was found to be a transducer consisting of two components, a linear spring with a matched fundamental frequency to the input and a linear viscous damper with the same damping coefficient as the parasitic mechanical losses. This example shows that the transducer architecture, previously assumed to be optimal in the literature and shown through numeric simulations to be unmatched in energy output, is in fact the optimal transducer for this input. This relationship has yet to have been explicitly proven.

The second application was for a vibration input of two sinusoids. The resulting optimal transducer, corresponding to the maximum energy output, was found to be a function of the separation factor between the two frequencies of the input. In general, this transducer is not realizable with a passive system. However, an upper bound on the energy output was determined and found to be twice that of the optimal transducer harvesting from a single sinusoid. The energy bound was also found not to be a function of the separation distance between the two input frequencies. An interesting result of this finding is that the upper energy bound is only a function of the lower of the two input frequencies. In all cases it was found that the optimal power transduction architecture was a linear viscous damper with matched impedance to the mechanical damping of the system. The portion of the

transducer force that was a function of the frequency separation was shown to be an energy conservative element acting only as a restoring force or spring for the system.

The final application of this framework was for a time varying input. The input was for a single sinusoid whose frequency changes linearly with time. This input is known as a sinusoid sweep or a chirp. The mathematical complexity of this application hindered directly finding an analytical solution. However, with the knowledge of the optimal transducer from the single stationary sinusoid, an optimal transducer for the swept sinusoid was assumed. This assumption was then checked against true optimal solution and found to converge quickly in time. The difference between the two signals was the addition of a transient to the assumed optimal solution. This transient was shown to decay quickly in time and converge to the optimal solution as found by the mathematical framework.

Based on the optimal transducer from the swept sinusoid input, a device was built and characterized. The characterization found that that the device remained linear through the actuation range, being tuned to a resonance frequency from 60-130 Hz. This system accurately represented the optimal transducer as found from the mathematical framework. From this application it was shown that the framework for finding the optimal transducer can be applied to the design of a real world system and used to validate a design's performance by giving a comparison to an upper limit for energy generated.

CHAPTER 9

FUTURE WORK

Continuation of this work could include examination of constrained and suboptimal solutions. These suboptimal solutions should be constrained in such a way, that the solutions represent realizable system, systems that can be represented as a function of their states, not as a function of time. A large assumption, which greatly affected the solution of the framework, was the form of the mechanical damping. Future work should investigate solutions that use different forms of mechanical damping, such as structural, or Coulomb damping.

The energy output from other works, such as Hoffmann's [6], should be compared to the theoretical maximum from this work. This will inform future researchers on the potential gains that can be made by using more complex architectures.

Finally, further work to the wishbone structure should be focused on developing an energy efficient control algorithm, rebuilding the device with a more compact actuator, and create an analytical solution relating the effective stiffness of the springs to the displacement between the bases of the two cantilever beams.

WORKS CITED

[1] S. Roundy, E. Leland, J. Baker and E. Carleton, "Improving Power Output for Vibration-Based Energy Scavengers," Energy Harvesting & Conservation, vol. 1536, no. 1268, pp. 28-36, 2005.

[2] S. Roundy, P. Wright and J. Rabaey, "A Study of Low Level Vibrations as a Power Source for Wireless Sensor Nodes," Computer Communications, vol. 26, no. 11, pp. 1131-1144, 2003.

[3] J. A. Paradiso and T. Starner, "Energy Scavenging for Mobile and Wireless Electronics," Energy Harvesting & Conservation, pp. 18-27, 2005.

[4] C. Williams, C. Shearwood, M. Harradine, P. Mellor, T. Birch and R. Yates, "Development of an Electromagnetic Microgenerator," Proc. Circuits Devices Syst., vol. 148, no. 6, pp. 337-342, 2001.

[5] G. K. Ottoman, H. F. Hofmann, A. C. Bhatt and G. A. Lesieutre, "Adaptive Piezoelectric Energy Harvesting Circuit for Wireless Remote Power Supply," Transactions on Power Electronics, vol. 17, no. 5, pp. 669-676, 2002.

[6] D. Hoffmann, B. Folkmer and Y. Manoli, "Comparative Study of Concepts for Increasing the Bandwidth of Vibration Based Energy Harvesters," PowerMEMS, 2012.

[7] B. Mann, D. Barton and B. Owens, "Uncertainty in Performance for Linear and Nonlinear Energy Harvesting Strategies," Intelligent Materials Systems and Structures, vol. 23, pp. 1451-1460, 2012.

[8] S. D. Nguyen, E. Halvorsen and I. Paprotny, "Bistable Springs for Wideband Microelectricmechanical Energy Harvesters," Applied Physics Letters, vol. 102, 2013.

[9] R. Ramlan, M. Brenan, B. Mace and I. Kovacic, "Potential Benefits of Noninear Stiffness in an Energy Harvesting Device," Nonlinear Dynamics, vol. 59, pp. 545-558, 2001.

[10] S. C. Stanton, C. C. McGehee and B. P. Mann, "Nonlinear Dynamics for Broadband Energy Harvesting: Investigation of a Bistable Piezoelectric Inertial Generator," Elservier Direct Science, 2010.

[11] B. P. Mann and B. Owens, "Investigations of a Nonlinear Energy Harvester With a Bistable Potential Well" Journal of Sound and Vibration, vol. 329, pp 1215-1226, 2010.

[12] J. Lynch and K. Loh, "A Summary Review of Wireless Sensors and Sensor Networks for Structural Health Monitoring," The Shock and Vibrations Digest, pp. 91 - 128, 2006.

[13] B. Mann, "Energy Harvesting from the Nonlinear Oscillation of Magnetic Levitation," Journal of Sound and Vibration, vol. 319, pp. 515-530, 2009.

[14] M. Mansour, M. Arafa and S. Hegahed, "Resonator with Magnetically Adjustable Natural Frequency for Vibration Energy Harvesting," Sensors and Actuators A: Physical, vol. 163, pp. 297-303, 2010.

[15] M. Daqaq, "Transduction of a Bistable Inductive Generator Driven by White and Exponentially Correlated Gaussian Noise," Journal of Sound and Vibration, vol. 330, pp. 2254-2564, 2010.

[16] A. E. Bryson and Y.-C. Ho, Applied Optimal Control, Hemisphere Publishing Corporation, 1975.

[17] A. Mukherjee, P. Mitcheson, E. Yeatman, D. Zhu and S. Beeby, "Magnetic Potential Well Tuning of Resonant Cantilever Energy Harvester," PowerMEMS, 2012.

[18] I. Ayala, D. Zhu, M. Tudor and S. Beeby, "Automonous Tunable Energy Harvester," PowerMEMS, pp. 49-52, 2009.

[19] V. R. Challa, M. G. Prasad, Y. Shi and F. T. Fisher, "A Vibration Energy Harvesting Device with Bidirectional Resonance Frequancy Tunability," Smart Materials and Structures, vol. 17, pp. 015035, 2008.

[20] C. Peters, "A Closed-Loop Wide-Range Tunable Mechanical Resonator for Energy Harvesting Systems, " Journal of Micromechanics and Microengineering, vol. 19, pp. 094004, 2009.

[21] L. S.-C. Huang and Kao-An, "A Novel Design of a Map-Tuning Piezoelectric Vibration Energy Harvester," Smart Materials and Structures, vol. 21, pp. 085014, 2012.

[22] C. Eichhorn, R. Tchagsim, N. Wilhelm and P. Woias, "A Smart and Self-Sufficient Frequency Tunable Vibration Energy Harvester," Journal of Micromechanics and Microengineering, vol. 21, pp. 104003, 2011.